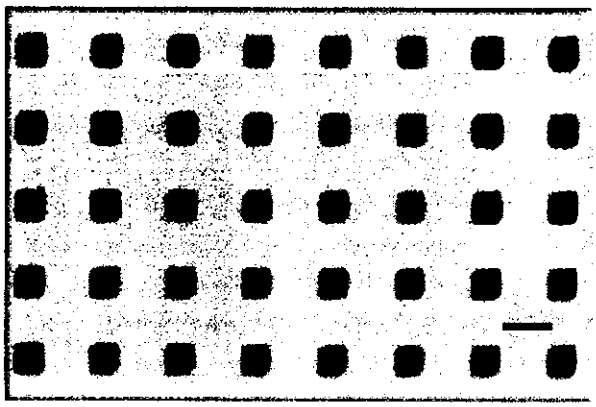

Figure 5. Microfluidic fidelity testing with three-dimensional PDMS microstructures. Fluorescent dye solution (1% rhodamine 123 in DMF) was poured onto the mold-glass sandwiched surface and observed under a microscope. No leaks were detected over all surfaces observed, reflecting high fidelity of pattern size and surface contact. Scale bar: 100 μm. [Color figure can be viewed in the online issue, which is available at www.interscience.wiley.com.]

Protein adsorption

FITC-labeled bovine serum albumin was dissolved in Dulbecco's phosphate buffered saline (PBS) at a concentration of 250 μg/mL. A few drops of the protein solution were distributed onto the PAAm-micropatterned surfaces and stored wet at room temperature overnight. The patterned surfaces were rinsed with PBS and water, and then directly examined under a fluorescence microscope (TE300; Nikon).

Cell culture

Bovine aortic endothelial cells (JCRB0099) were provided from Japan Health Science Foundation and cultured in Dulbecco's modified Eagle minimum essential medium (DMEM) supplemented with 10% fetal bovine serum (FBS), 100 U/mL penicillin and 100 μg/mL streptomycin. Cells were recovered from tissue culture polystyrene dishes by treatment with 0.05% trypsin/0.05% ethylenediaminetetraacetic acid in PBS and were routinely split at a ratio of 1:4 and carried in DMEM supplemented with 10% FBS, 100 U/mL penicillin, and 100 μg/mL streptomycin. Endothelial cells (5.0×10^4 cells/mL) were seeded onto treated glass coverslips. Cell morphology in culture on patterned surfaces was monitored under a phase contrast microscope (TE300; Nikon).

RESULTS

In the present study, reliable surface micropatterning to produce cell-surface manipulations was achieved in two steps (shown in Fig. 1). First, three-

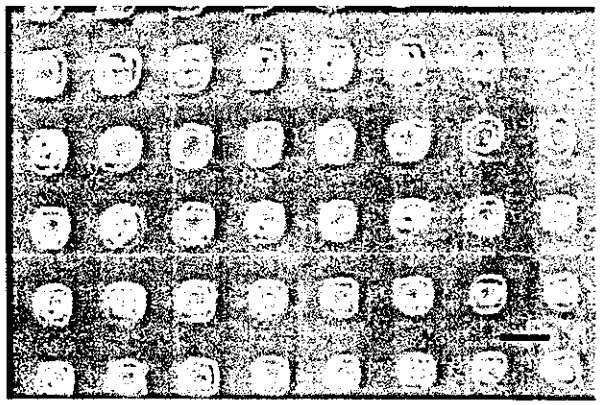

Figure 6. Water condensation patterns on PAAm-micropatterned surfaces seen in phase contrast microscopy. Scale bar: 100 μm.

dimensional molded microstructures were prepared with PDMS on silanized glass surfaces by photopolymerization utilizing the LCDP-modified device. In the modified LCDP used in the present study, light from the lamp passed through liquid crystal panels was downsized by the projector lens, turned by the beam splitter downward, and irradiated onto the sample stage, whose position was monitored and controlled for focus adjustment. The LCDP used here has three liquid crystal panels each comprising 480,000 pixels (800 × 600, 1.78 cm in diagonal). Each square pixel has sides of 18 μm reduced through the projection lens optics. In the present study, the reduced individual pixel size was fixed to 10 μm, so that the final projection area was 8 × 6 mm. Mask patterns were generated on a typical PC with commercially available software such as Microsoft Word® and Microsoft PowerPoint®. Identical images appearing on the PC monitor were projected onto the sample stage in a reduced size. After photopolymerization, the resultant

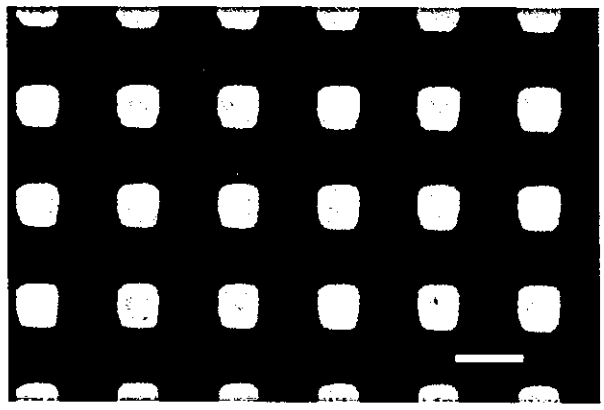

Figure 7. FITC-albumin adsorption on PAAm-micropatterned surfaces detected with fluorescent microscopy. Scale bar: 100 μm. [Color figure can be viewed in the online issue, which is available at www.interscience.wiley.com.]

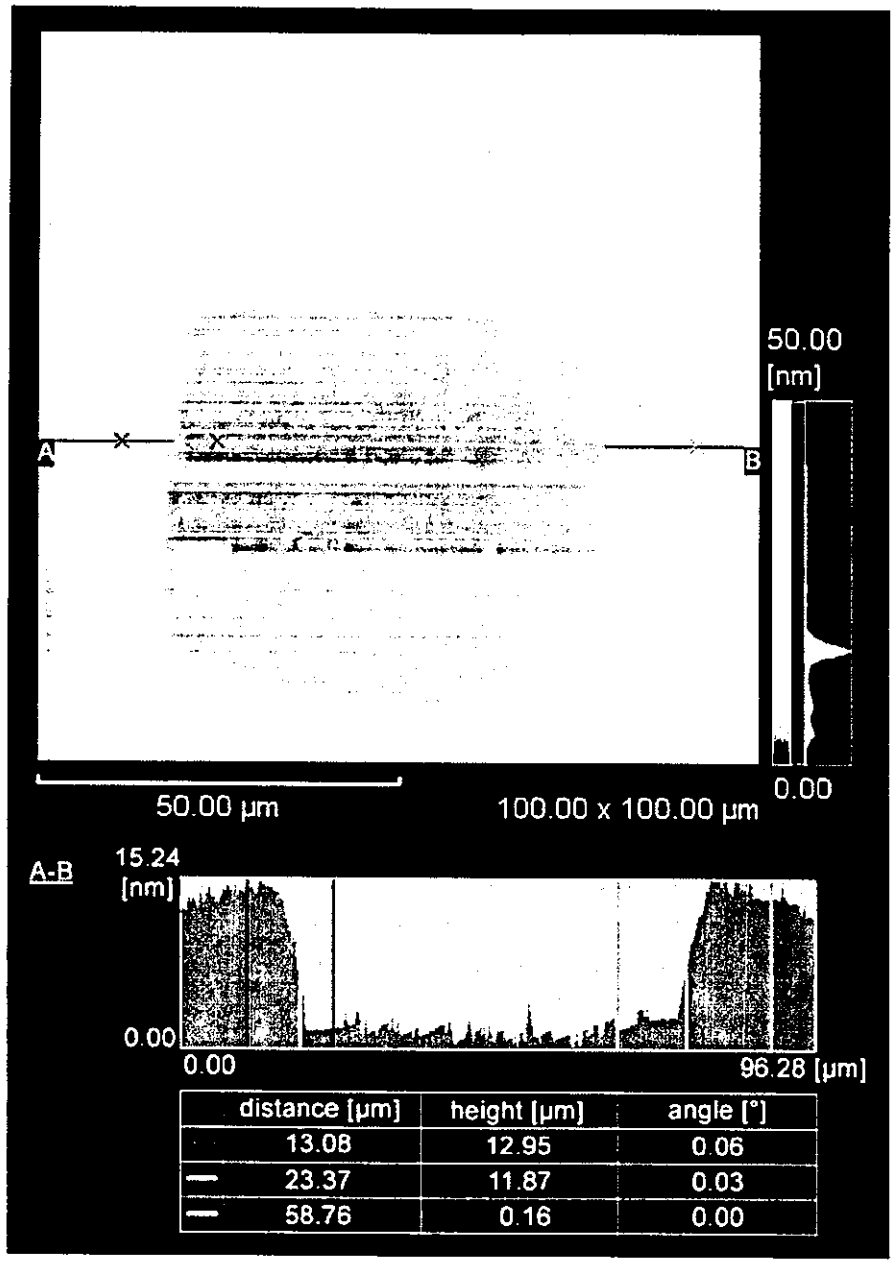

Figure 8. Three-dimensional profiles of wet PAAm-micropatterned surfaces observed with AFM.

three-dimensional PDMS microstructures are easily observed under a phase contrast microscope (see Fig. 2) as well as by SEM (shown in Fig. 3). Three-dimensional topological profiles were obtained with a reflective confocal laser scanning microscope (images shown in Fig. 4). As these imaging methods show, high fidelity to the computer-generated mask patterns was consistently achieved. The convex and concave domains corresponded to white and black domains on PC-generated images, respectively. Under the present conditions, the depth of concave domains is approximately 2 µm, but the sectional sidewall profile was trapezoidal. The top had the same dimension as the PC-generated images, whereas the base of the structure formed was slightly larger. This is likely caused by LCD light scattering and/or diffraction. Each micropattern comprised small square dots having 10-µm sides. Because of shading from LCD wires aligned between pixels on the liquid crystal panel to switch each pixel on and off, small submicron gaps were formed by LCD exposure among square dots [arrow in Fig. 2(b)].

These three-dimensional PDMS microstructures were directly pressed onto another silanized glass sur-

Figure 9. Cell manipulation on PAAm-micropatterned surfaces (phase contrast microscope image after culture in 10% FBS-DMEM for 19 days). Scale bar: 100 μm (left); 50 μm (right).

face, forming molded patterned channels on contact for microfluidics purposes. To confirm tight contact of PDMS microstructures on these glass surfaces, rhodamine DMF dye solution was flowed around these contacts and observed under a microscope (shown in Fig. 5). No leaks were detected over the entire surfaces observed, so that quite a sharp, fluid-tight boundary between the concave and convex PDMS domains was obtained. Acrylamide monomer solution was then poured through these concave microstructures, and light was irradiated. Photopolymerization of acrylamide occurred only in the concave-molded domains, so that surface micropatterning with hydrophilic PAAm could be achieved using the patterned PDMS template. After polymerization of PAAm, the resultant polymer micropattern was not detected under a phase contrast microscope, but the surface micropatterning was visualized by two other ways. First, water vapor condensation was observed only on non-PDMS contact areas under a humid atmosphere (see Fig. 6). Because silanized glass surfaces are hydrophobic, condensation is expected to occur selectively on hydrophilic PAAm surfaces.[11] Second, FITC-albumin adsorption was observed only in the areas contacted directly by the PDMS convex patterns during acrylamide photopolymerization (see Fig. 7). Hydrophilic PAAm surfaces are known to repel protein adsorption,[12,13] consistent with these observations and pattern fidelity. Wet PAAm layer thickness was determined to be approximately 12 nm by AFM (see Fig. 8).

On the micropatterned surfaces, endothelial cells specifically adhered to patterned areas where the PDMS convex domains contacted the silanized surface, that is, where PAAm could not flow or be photografted (see images in Fig. 9). Such site-selective cell adhesion was achieved even in the presence of 10% FBS media. Consistently, on the areas not in contact with the PDMS patterns (i.e., channel domains where PAAm was grafted), cell adhesion was completely inhibited. The cell micropattern fidelity was maintained intact for more than 1 month even in the presence of serum (data not shown). Cytotoxicity was not observed during this culture (data not shown).

DISCUSSION

In our previous study, one-step LCD micropatterning of surfaces by grafting with polyethylene glycol was reported.[10] Liquid crystal panels equipped in the projector can completely shield emitted light to pattern at high line resolution. However, irradiated light can be diffracted or scattered on the glass surface substrate and diffused through the glass. Therefore, polyethylene glycol was found to be grafted even on black (unexposed) domains in PC-generated images. To eliminate the effect of light diffraction and scattering for more precise control of surface micropatterning, two-step micropatterning has been developed here. Because the PDMS molds exhibited tight contacts with silanized glass surfaces, no liquid leakage was observed from the microfluidic tests of sealing. Therefore, a high fidelity of final PAAm micropatterns with the top surface image transfer from the PDMS molds was obtained.

Under the present conditions, the resultant PAAm layers were highly hydrophilic and able to repel protein adsorption (see Fig. 7). On the contrary, silanized glass surfaces allowed cell adhesion in culture medium supplemented with serum even without precoating extracellular matrix proteins such as fibronectin, typically required for cell adhesion on hydrophobic surfaces. As a result, selective cell adhesion at high pattern fidelity was achieved by cell seeding on micropatterned surfaces in the presence of serum (Fig. 9).

Micropatterned surfaces were fabricated easily and quickly with the present LCD device without any need for expensive pattern mask masters, an additional light source, or other optics. Even with the present typical LCDP, requisite pattern fidelity and

resolution for many biomedical applications is readily achievable. Recent progress in improved high resolution and high-density LCDP will facilitate much finer micropatterning required for more advanced applications. The present device has both a liquid crystal panel imaging PC-generated patterns and an intense light source. Such an all-in-one device should be useful for the preparation of micropatterned surfaces for biomedical applications and other microfluidics surfaces in a rapid prototyping manner.

The authors appreciate the useful comments and technical criticism from Prof. D. W. Grainger (Colorado State University, Fort Collins, CO). The authors are grateful to Mr. Masao Matsuda of Shimadzu Corporation for AFM experiments, and are thankful for the cooperation of Digital Systems Development Center of Sanyo Electric Co., Ltd.

References

1. Xia Y, Whitesides GM. Soft lithography. Angew Chem Int Ed Engl 1998;37:550–575.
2. Whitesides GM, Ostuni E, Takayama S, Jiang X, Ingber DE. Soft lithography in biology and biochemistry. Annu Rev Biomed Eng 2001;3:335–373.
3. Michel B, Bernard A, Bietsch A, Delamarche E, Geissler M, Juncker D, Kind H, Renault J-P, Rothuizen H, Schmid H, Schmidt-Winkel P, Stutz R, Wolf H. Printing meets lithography: soft approaches to high-resolution patterning. IBM J Res Dev 2001;45:697–719.
4. Grzybowski BA, Haag R, Bowden N, Whitesides GM. Generation of micrometer-sized patterns for microanalytical applications using a laser direct-write method and microcontact printing. Anal Chem 1998;70:4645–4652.
5. Wolfe DB, Ashcom JB, Hwang JC, Schaffer CB, Mazur E, Whitesides GM. Customization of poly(dimethylsiloxane) stamps by micromachining using a femtosecond-pulsed laser. Adv Mater 2003;15:62–65.
6. Qin D, Xia Y, Whitesides GM. Rapid prototyping of complex structures with feature sizes lager than 20 μm. Adv Mater 1996;8:917–919.
7. McDonald JC, Whitesides GM. Poly(dimethylsiloxane) as a material for fabricating microfluidic devices. Acc Chem Res 2002;35:491–499.
8. Beebe DJ, Moore JS, Bauer JM, Yu Q, Liu RH, Devadoss C, Jo B-H. Functional hydrogel structures for autonomous flow control inside microfluidic channels. Nature 2000;404:588–590.
9. Wong JY, Velasco A, Rajagopalan P, Pham Q. Directed movement of vascular smooth muscle cells on gradient-compliant hydrogels. Langmuir 2003;19:1908–1913.
10. Itoga K, Yamato M, Kobayashi J, Kikuchi A, Okano T. Cell micropatterning using photopolymerization with a liquid crystal device commercial projector. Biomaterials 2004;25(11):2047–2053.
11. Ionov L, Minko S, Manfred Stamm M, Gohy J-F, Jérôme R, Scholl A. Reversible chemical patterning on stimuli-responsive polymer film: environment-responsive lithography. J Am Chem Soc 2003;125:8302–8306.
12. Bearinger JP, Castner DG, Golledge SL, Rezania A, Hubchak S, Healy KE. P(AAm-*co*-EG) interpenetrating polymer networks grafted to oxide surfaces: surface characterization, protein adsorption, and cell detachment studies. Langmuir 1997;13:5175–5183.
13. Saito N, Matsuda T. Protein adsorption on self-assembled monolayers with water-soluble non-ionic oligomers using quartz-crystal microbalance. Mater Sci Eng C 1998;6:261–266.

Ultrathin Poly(*N*-isopropylacrylamide) Grafted Layer on Polystyrene Surfaces for Cell Adhesion/Detachment Control

Yoshikatsu Akiyama,† Akihiko Kikuchi,† Masayuki Yamato,† and Teruo Okano*,†

Institute of Advanced Biomedical Engineering and Science, COE Program for 21st Century, Tokyo Women's Medical University, 8-1 Kawadacho, Shinjuku-ku, Tokyo 162-8666, Japan

Received November 14, 2003. In Final Form: April 12, 2004

We investigated physicochemical properties of two types of poly(*N*-isopropylacrylamide) (PIPAAm)-grafted tissue culture polystyrene (TCPS) surfaces, to elucidate the influential factors for thermally regulated cell adhesion and detachment to PIPAAm-grafted surfaces. The two types of PIPAAm-grafted surfaces were prepared by the electron beam polymerization method. Attenuated total reflection Fourier transform infrared spectroscopy revealed that amounts of the grafted polymers were $1.4 \pm 0.1\ \mu g/cm^2$ for PIPAAm-1.4 and $2.9 \pm 0.1\ \mu g/cm^2$ for PIPAAm-2.9. Both PIPAAm-grafted surfaces showed hydrophobic/hydrophilic property alterations in response to temperature. However, PIPAAm-1.4 surfaces were more hydrophobic ($\cos\theta = 0.21$ at 37 °C and $\cos\theta = 0.35$ at 20 °C) than PIPAAm-2.9 ($\cos\theta = 0.42$ at 37 °C and $\cos\theta = 0.50$ at 20 °C) both above and below the PIPAAm's transition temperature. Thicknesses of the grafted PIPAAm layers were estimated to be 15.5 ± 7.2 nm for PIPAAm-1.4 and 29.5 ± 8.4 nm for PIPAAm-2.9, by the use of UV excimer laser and atomic force microscope. Bovine carotid artery endothelial cells (ECs) adhere to the surfaces of PIPAAm-1.4 and proliferate to form confluent cell monolayers. The cell monolayers were harvested as single cell sheets by temperature decrease from 37 to 20 °C. On the contrary, ECs did not adhere to the surfaces of PIPAAm-2.9. This phenomenon was correlated with an adsorption of cell adhesion protein, fibronectin, onto surfaces of PIPAAm-1.4 and -2.9. In the case of nano-ordered thin grafted surfaces, the surface chain mobility is strongly influenced by the thickness of PIPAAm grafted layers because dehydration of PIPAAm chains should be enhanced by the hydrophobic TCPS surfaces. PIPAAm graft amounts, that is, thickness of the PIPAAm grafted layers, play a crucial role in temperature-induced hydrophilic/hydrophobic property alterations and cell adhesion/detachment behavior.

Introduction

We have been carrying out the preparation of thermoresponsive polymer-modified surfaces with designated molecular configuration at the interfaces.[1-3] Thermoresponsive polymers poly(*N*-isopropylacrylamide) (PIPAAm) and its derivatives are used as the surface modifiers.[1-3] These surfaces are utilized to propose new chromatographic separation methods for a variety of types of bioactive compounds in a sole aqueous mobile phase.[4-6] We further applied the thermoresponsive surfaces for thermally regulated cell adhesion and detachment[7-9] and extended the idea to tissue engineering.[10-13] Confluently cultured cell monolayers on hydrophobized PIPAAm-modified surfaces at 37 °C detach as single cell sheets by lowering the culture temperature to 20 °C where the modified surfaces become hydrophilic due to PIPAAm's hydration/dehydration transition at 32 °C. In our preliminary studies, graft amounts of PIPAAm on the surfaces have significant influence on cell adhesion behavior.[14,15] However, detailed mechanisms to explain why cells cannot adhere on the surfaces with high amounts of grafted PIPAAm chains are unclear. Such phenomenon was also found for PIPAAm dip-coated surfaces or PPAAm hydrogels.

In the present paper, we focused on the correlation of the thickness of PIPAAm covalently grafted layers on tissue culture polystyrene (TCPS) surfaces and cell adhesion/detachment behavior. For this purpose, we utilized limited excimer laser ablation and atomic force microscopic methods to determine the thickness of PIPAAm grafted layers. Preliminary ellipsometry measurement did not work to determine the grafted layer thickness, since the refractive indices are similar for polystyrene and PIPAAm. Then, we investigated thermoresponsive

* Corresponding author. Phone: +81-3-3353-8111 ext. 30233. Fax: +81-3-3359-6046. E-mail: tokano@abmes.twmu.ac.jp.

† Core Researches for Evolutional Science and Technology (CREST), Japan Science and Technology Agency.

(1) Takei, Y. G.; Aoki, T.; Sanui, K.; Ogata, N.; Sakurai, Y.; Okano, T. *Macromolecules* **1994**, *27*, 6163−6166.

(2) Yakushiji, T.; Sakai, K.; Kikuchi, A.; Aoyagi, T.; Sakurai, Y.; Okano, T. *Langmuir* **1998**, *14*, 4657−4662.

(3) Kikuchi, A.; Okano, T. *Prog. Polym. Sci.* **2002**, *27*, 1165−1193.

(4) Kanazawa, H.; Yamamoto, K.; Matsushima, Y.; Takai, N.; Kikuchi, A.; Sakurai, Y.; Okano, T. *Anal. Chem.* **1996**, *68*, 100−105.

(5) Kanazawa, H.; Kashiwase, Y.; Yamamoto, K.; Matsushima, Y.; Kikuchi, A.; Sakurai, Y.; Okano, T. *Anal. Chem.* **1997**, *69*, 823−830.

(6) Kanazawa, H.; Sunamoto, T.; Matsushima, Y.; Kikuchi, A.; Sakurai, Y.; Okano, T. *Anal. Chem.* **2000**, *72*, 5961−5966.

(7) Yamada, N.; Okano, T.; Sakai, H.; Karikusa, F.; Sakurai, Y. *Makromol. Chem. Rapid. Commun.* **1990**, *11*, 571−576.

(8) Okano, T.; Yamada, N.; Sakai, H.; Sakurai, Y. *J. Biomed. Mater. Res.* **1993**, *27*, 1243−1251.

(9) von Recum, H. A.; Kim, S. W.; Kikuchi, A.; Okuhara, M.; Sakurai, Y.; Okano, T. *J. Biomater. Sci., Polym. Ed.* **1998**, *9*, 1241−1254.

(10) Kushida, A.; Yamato, M.; Konno, C.; Kikuchi, A.; Sakurai, Y.; Okano, T. *J. Biomed. Mater. Res.* **2000**, *51*, 216−223.

(11) Shimizu, T.; Yamato, M.; Kikuchi, A.; Okano, T. *Tissue Eng.* **2001**, *7*, 141−151.

(12) Yamato, M.; Shimizu, T.; Harimoto, M.; Hirose, M.; Kushida, A.; Kwon O. H.; Kikuchi, A.; Okano, T. In *Tissue Engineering for Therapeutic Use 5*; Ikada, Y., Ohshima, N., Eds.; Elsevier Science: Amsterdam, 2001; pp 93−100.

(13) Yamato, M.; Okano, T. *Macromol. Chem. Symp.* **2001**, *14* (2), 21−29.

(14) Sakai, H.; Doi, Y.; Okano, T.; Yamada, N.; Sakurai, Y. In *Advanced Biomaterials In Biomedical Engineering and Drug Delivery Systems*; Ogata, N., Feijen, J., Kim, S. W., Okano, T., Eds.; Springer: Tokyo, 1996; pp 229−230.

(15) Yamato, M.; Konno, C.; Koike, S.; Isoi, Y.; Shimizu, T.; Kikuchi, A.; Makino, K.; Okano, T. *J. Biomed. Mater. Res.* **2003**, *67A*, 1065−1071.

10.1021/la036139f CCC: $27.50
Published on Web 05/26/2004

cellular adhesion/detachment on the prepared surfaces to discuss the influence of the grafted layer thickness on the cellular behavior on these modified surfaces.

Experimental Section

Preparation of the PIPAAm-Grafted TCPS Dishes. PIPAAm-grafted surfaces were prepared as reported previously.[4] In brief, *N*-isopropylacrylamide (IPAAm) monomer, a kind gift from Kohjin (Tokyo, Japan), was dissolved in 2-propanol at concentrations of 55 and 80 wt %. Solution (30 μL) was added and spread uniformly over TCPS surfaces (Falcon 3001, BD Bioscience, Billerica, MA) These dishes were immediately subjected to irradiation with a 0.25 MGy electron beam, using an Area Beam Electron Processing System (Nissin High Voltage, Kyoto, Japan). PIPAAm-grafted dishes were washed extensively with cold distilled water to remove unreacted IPAAm monomer and ungrafted PIPAAm.

Preparation of PIPAAm-Grafted Gel on Glass Coverslips. IPAAm monomer (1.56 g), *N,N*-methylenebisacrylamide (27 mg), and ammonium peroxodisulfate (8.0 mg) were dissolved in distilled water (10 mL). The mixture was subject to N_2 bubbling for 10 min and then *N,N,N',N'*-tetramethylethylenediamine (48 μL) was added to the mixture. The mixture was immediately poured into the void space between two glass coverslips where a Teflon spacer (with 50 μm thickness) was placed. In advance, the coverslip surfaces were modified with 3-methacryloxypropyl trimethoxysilane after O_2 plasma treatment. Polymerization reaction for the glass coverslips containing the mixture was performed at 15 °C for 24 h, and the resulting grafted PIPAAm gel was washed extensively with distilled water.

UV Excimer Laser Ablation of PIPAAm-Grafted Surfaces. Irradiation of an ArF excimer laser (L5910 III B; Hamamatsu Photonics K.K., Shizuoka, Japan) was achieved onto PIPAAm-grafted surfaces by passing a laser pulse through an optical microscope, resulting in ablative photodecomposition. The excimer laser (193 nm) was irradiated at a laser fluence of either 10 or 20 mJ/cm^2 with a pulse width of 5 ns. The number of laser shots was changed from 1 to 9 onto the PIPAAm-grafted surfaces. Each ablated region was 30 μm × 25 μm.

Staining PIPAAm-Grafted Surfaces with Hydrophobic Fluorescent Dye, DiIC18. The laser-ablated surfaces were stained with 25 μg/mL 1,1'-dioctadecyl-3,3,3',3'-tetramethylindocarbocyanine perchlorate (DiIC18) (Molecular Probes Inc., Eugene, OR) in Dulbecco's phosphate-buffered saline (PBS; Sigma, St. Louis, MO) for 1 min at 23 °C. They were then washed extensively with PBS for five times. The surfaces were finally observed by fluorescent microscope. The fluorescence intensity of the ablated surfaces was evaluated by NIH image software (for the Macintosh, version 1.63).

Characterization. The amount of grafted PIPAAm was determined by attenuated total reflection Fourier transform infrared spectroscopy (ATR/FTIR, IR-470 Plus equipped with an ATR-300 H unit (Ge crystal with an incidence angle of 45°, and the number of reflection of 8; JASCO Co., Tokyo, Japan). As the base substrate was TCPS, an absorption arising from monosubstituted aromatic rings was observed at 1600 cm^{-1}. Absorption of amide carbonyl derived from PIPAAm grafts appeared in the region of 1650 cm^{-1}. The peak intensity ratio of I_{1650}/I_{1600} was used to determine the graft density of PIPAAm on the surfaces. A known PIPAAm amount cast on TCPS from solution was used for a calibration curve. Surface wettability was evaluated by measuring static contact angles (Image processing type CA-X, Kyowa Interface Science, Saitama, Japan) toward air bubbles in Milli-Q water. Atomic force microscopy (AFM) images were obtained with a NanoScope IIIa (Digital Instruments, Santa Barbara, CA) using Tapping Mode in air, for measuring the thickness of the grafted polymer layers. Prior to measurements, the central part of PIPAAm-grafted dishes was cut into a piece of 1 cm × 1 cm in size. The scan rate was 0.2 Hz, and the measurements were carried out with an AFM probe of NCHW type (NANOSENSORS, Germany). The rms (root-mean-square) value of the surface roughness of the image was determined with software supplied with the NanoScope IIIa. The thickness of the grafted polymer layers was determined from data of section profiles drawn in the AFM image. Time-of-flight secondary ion mass spectrometry (TOF-SIMS) images were obtained with a TOF-SIMS IV (Cameca Instruments, France) system in static mode. The dose of gallium ions used as the primary beam was 1.9×10^{13} ions/cm^2.

Cells and Cell Culture. Bovine endothelial cells (ECs; Health Science Research Resource Bank, Osaka, Japan) were cultured with Dulbecco's modified Eagle's medium (DMEM; IWAKI, Chiba, Japan) supplemented with 10% fetal bovine serum (FBS; MORGATE Co., Ltd., Bulimba, Australia), 100 units/mL penicillin, 100 μg/mL streptomycin, and 0.25 μg/mL fungizone at 37 °C in a humidified atmosphere with 5.0% CO_2. ECs were recovered from normal TCPS dishes by treatment with 0.25% trypsin–2.65 mM EDTA (GIBCO BRL Life Technologies, Grand Island, NY) in PBS and seeded on PIPAAm-grafted dishes having different PIPAAm graft densities and TCPS dishes as the reference at 1.3×10^4 cells/cm^2. Cell morphology was photographed under a phase contrast microscope (TE300, Nikon, Tokyo, Japan).

Fibronectin Adsorption onto PIPAAm-Grafted Surfaces. Bovine plasma fibronectin (FN; Biomedical Technology Inc., Stoughton, MA) was adsorbed onto the PIPAAm-grafted surfaces by incubation of 10 μg/mL FN in PBS solution at 37 °C for 6 h. These dishes were then vigorously washed with PBS for five times. They were then blocked with 0.1% bovine serum albumin (BSA) in PBS for 1 h and reacted with 2.0 mg/mL rabbit polyclonal anti-bovine FN antibody (Biogenesis, Inc., Poole, U.K.) at a 1:200 dilution (final concentration, 10 μg/mL) for 2 h at 23 °C. Following five washes with PBS containing 0.1% BSA, they were incubated for an additional 1 h with 3.0 mg/mL FITC-conjugated goat anti-rabbit IgG antibody (CHEMICON International, Inc., Temecula, CA) with a 1:200 dilution (final concentration, 15 μg/mL) and again washed vigorously with 0.1% BSA in PBS for five times. The stained dishes were observed with a fluorescent microscope (TE2000-U, Nikon). After adsorption of FN molecules, the FN solution was collected and the concentration of FN was estimated by the micro BCA assay method (PIERCE Biotechnology, Inc., Rockford, IL). Amounts of adsorbed FN on PIPAAm-1.4, PIPAAm-2.9, and control TCPS surfaces were estimated from the calibration curve.

Results

Characterization of PIPAAm-Grafted Surfaces. Here, two types of PIPAAm-grafted TCPSs were evaluated for graft amounts of the PIPAAm surfaces and their thermoresponsive wettability changes. The grafted polymer amounts on two PIPAAm-grafted surfaces were determined from ATR/FTIR measurements and were 1.4 ± 0.1 μg/cm^2 (n = 4) and 2.9 ± 0.1 μg/cm^2 (n = 4), respectively. Those two surface types are abbreviated as PIPAAm-1.4 and PIPAAm-2.9, respectively, hereafter. Surface wettability of PIPAAm-1.4 and -2.9 was altered with temperature, as $\cos\theta = 0.21 \pm 0.01$ ($\theta = 77.9 \pm 0.60°$) ($n = 3$) for PIPAAm-1.4 and $\cos\theta = 0.35 \pm 0.02$ ($\theta = 69.5 \pm 1.20°$) ($n = 3$) for PIPAAm-2.9 at 37 °C changed to $\cos\theta = 0.42 \pm 0.02$ ($\theta = 65.2 \pm 1.20°$) ($n = 3$) for PIPAAm-1.4 and $\cos\theta = 0.50 \pm 0.01$ ($\theta = 60.0 \pm 0.06°$) ($n = 3$) for PIPAAm-2.9 at 20 °C.

Grafted PIPAAm Layers on TCPS Surfaces by UV Laser Ablation. PIPAAm-grafted TCPS surfaces were ablated with the UV excimer laser until the TCPS region was exposed for the following measurement of the graft layer thickness by means of atomic force microscopy. The ablated domains were stained with a hydrophobic fluorescent dye, DiIC18, to see whether the hydrophobic TCPS regions were exposed. Fluorescence of ablated domains was scarcely seen at one laser shot (Figure 1a). By sharp contrast, the fluorescent dye selectively stained the ablated domains clearly with increasing number of laser shots. The fluorescent intensity for PIPAAm-1.4 is likely to be saturated with 6 laser shots as shown in Figure 1b. This result indicates that the TCPS region is successfully exposed by 6 times of the laser ablation.

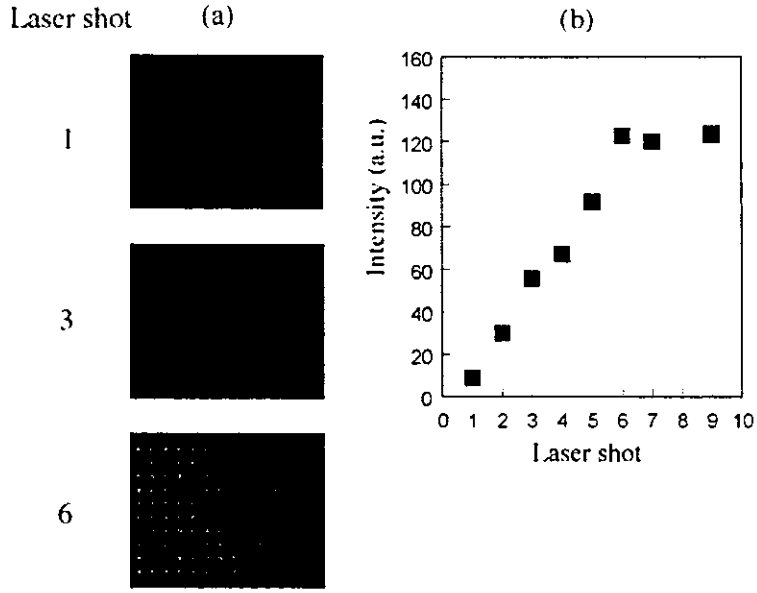

Figure 1. Fluorescence images of the domains on PIPAAm-1.4 surfaces stained by DiIC18 after the UV laser ablation at the number of 1, 3, and 6 laser shots (a) and fluorescence intensity of the domain as a function of the number of UV excimer laser shots (b). The numbers inserted in the fluorescent images correspond to the number of the laser shot. The laser fluence for the squares was 10 mJ/cm^2.

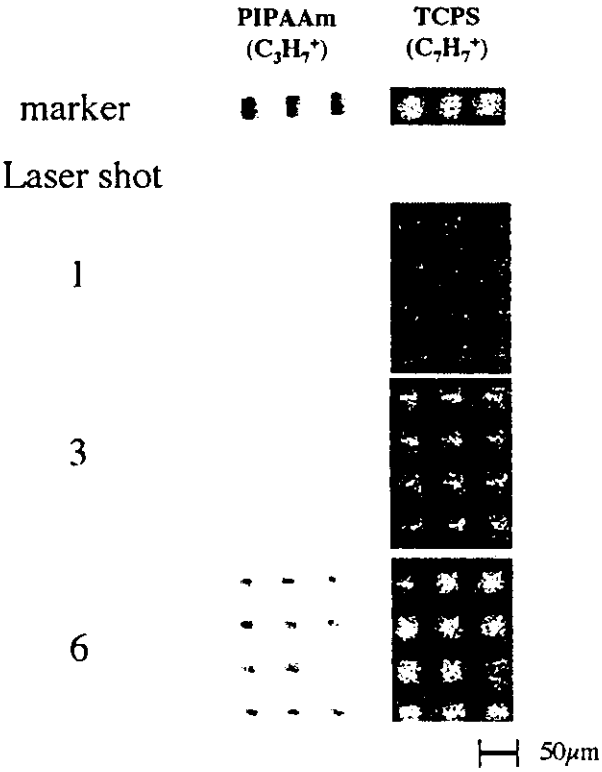

Figure 2. TOF-SIMS images displayed the spatial distribution of $C_3H_7^-$ (left) and $C_7H_7^-$ species (right) on PIPAAm-1.4 surfaces after the UV laser ablation at the number of 1, 3, and 6 laser shots. These images correspond to the images shown in Figure 1a. The $C_3H_7^-$ and $C_7H_7^-$ are characteristic of ion fragments derived from PIPAAm and TCPS composition, respectively. The laser fluence for the marker areas in the images was 50 mJ/cm^2.

Such a gradual exposure of TCPS was further confirmed by TOF-SIMS measurements (Figure 2). $C_3H_7^-$ ion was used to assign PIPAAm isopropyl side groups, and $C_7H_7^-$ ion was for phenyl groups of TCPS. In the left column of Figure 2, the entire surface was in bright color except the marker regions at laser shot of 1. With increasing laser shots, darker regions were seen in $C_3H_7^-$ ions. Such regions were brighter as $C_7H_7^-$ ion species were chosen in the TOF-SIMS images (right column in Figure 2).

Likewise, the ablated areas were stained with the fluorescent dye on PIPAAm-2.9 surfaces after the laser ablation. A stronger laser fluence was necessary for staining the regions (Figure 3), while such images were not obtained at a laser shot of 1 or 2 (data not shown). The stronger fluence should be due to the different amount and thickness of the grafted PIPAAm layers. The fluorescence intensity saturation at the laser shot of 3 also indicates that the TCPS region is completely revealed at this condition.

Measurement of Thickness of PIPAAm Layers by AFM. Figure 4 shows AFM images and their section profiles of the ablated domains for PIPAAm-1.4 (a) and for PIPAAm-2.9 (b). The PIPAAm-1.4 surface was relatively smooth, and ablated areas were clearly observed. This is sharp contrast with the relatively rough PIPAAm-2.9 surface. The rms values of PIPAAm-1.4 and -2.9 surfaces before the laser ablation were approximately 7.7 and 16.5 nm (data not shown), while those of the nonablated area in Figure 4a,b were ca. 6.0 and 17.2 nm, respectively. Equivalent rms values before and after laser ablation indicate that the laser ablation with 10 and 20 mJ/cm^2 did not contaminate surfaces of PIPAAm-1.4 and -2.9 with ablated debris. Section profiles showed the depth to be 15.5 ± 7.2 nm, indicating the thickness of the grafted PIPAAm layer for PIPAAm-1.4. Likewise, the averaged thickness of PIPAAm grafted layers for PIPAAm-2.9 was 29.3 ± 8.4 nm. Considering the amount and density of the grafted polymer on PIPAAm-1.4 and -2.9, thicknesses of the grafted polymer layers are reasonable.

Cell Adhesion and Detachment Changes on PIPAAm-Grafted Surfaces. Immunofluorescent staining against adsorbed FN was carried out on the surfaces of the PIPAAm-1.4, PIPAAm-2.9, and PIPAAm gel grafted (50 μm thick) glass coverslips (abbreviated as PIPAAm-

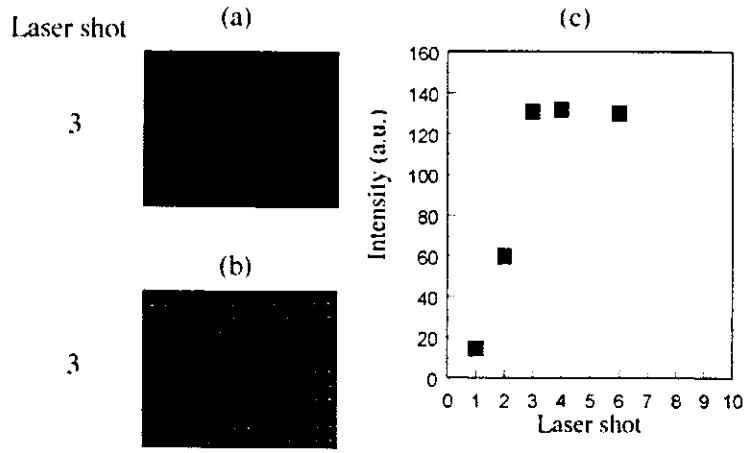

Figure 3. Fluorescence images of the squares on PIPAAm-2.9 surfaces stained by DiIC18 after the UV laser ablation at 10 mJ/cm² (a) and at 20 mJ/cm² (b) for three times. Fluorescence intensity of the domain as a function of the number of UV excimer laser shots at 20 mJ/cm² (c).

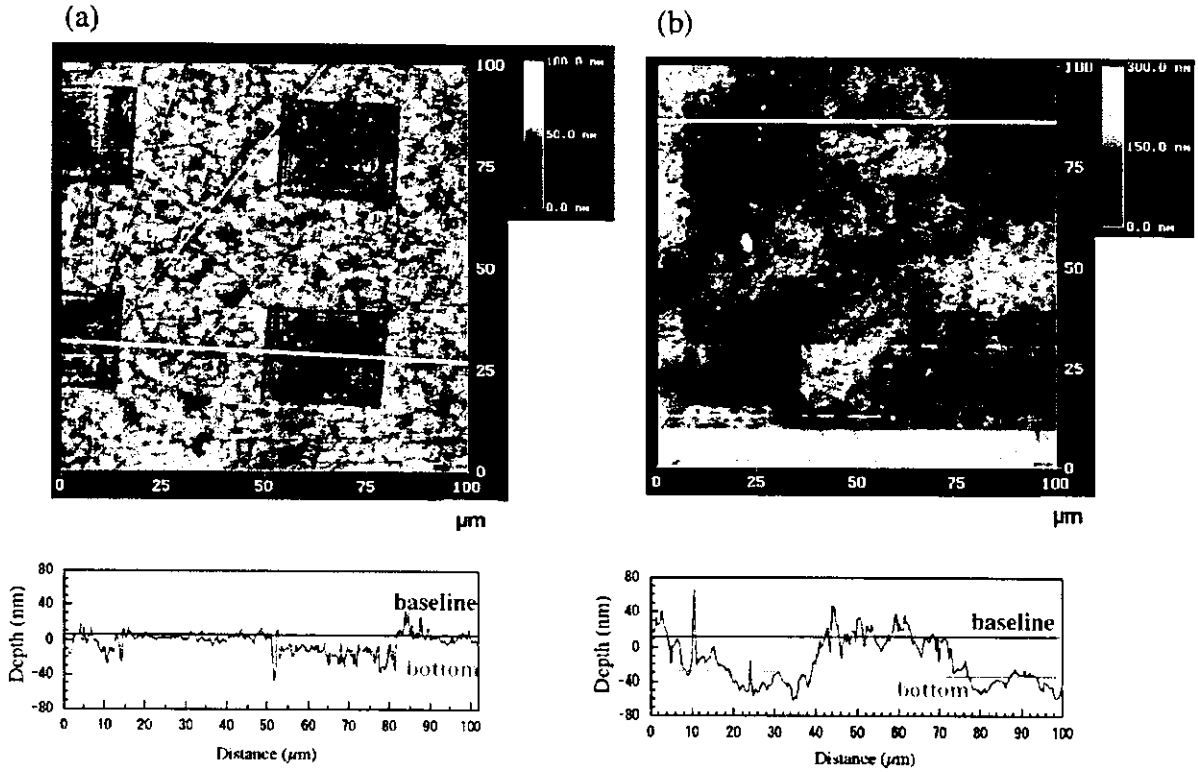

Figure 4. Tapping mode AFM observation for the laser-ablated domains on PIPAAm-1.4 (a) and PIPAAm-2.9 surfaces (b). The laser fluence and the number of irradiations were 10 mJ/cm² and 6 for PIPAAm-1.4 (a) and 20 mJ/cm² and 3 for PIPAAm-2.9 (b). The baseline and the bottom were averages of the text data from the section profiles (see Experimental Section). The scan size was 100 μm × 100 μm.

50). Fluorescence images revealed that FN adsorbed on the surfaces of PIPAAm-1.4. This is in good agreement with a previous report[16] that PIPAAm-modified surfaces with almost the same graft amount showed homogeneous FN adsorption at 37 °C. However, such FN adsorption was not observed on hydrophilic PIPAAm-grafted surfaces at 20 °C.[16] On the other hand, the immunofluorescent images for PIPAAm-2.9 and -50 were not as apparent as that for PIPAAm-1.4, meaning that adsorption of FN for PIPAAm-2.9 and -50 surfaces is negligible. Adsorbed FN for PIPAAm-1.4 and TCPS surfaces was estimated to be approximately 150 and 350 ng/cm², respectively. The amount of the adsorbed FN should be reasonable for ECs to adhere on the PIPAAm-1.4 surfaces,[17] while the estimated value for TCPS is comparable to that of the previous report.[18]

(16) Yamato, M.; Konno, C.; Kushida, A.; Hirose, M.; Utsumi, M.; Kikuchi, A.; Okano, T. *Biomaterials* **2000**, *21*, 981–986.

(17) Iuliano, D. J.; Saavedra, S. S.; Truskey, G. A. *J. Biomed. Mater. Res.* **1993**, *27*, 1103–1113.

(18) García, A. J.; Vega, M. D.; Boettiger, D. *Mol. Biol. Cell* **1999**, *10*, 785–798.

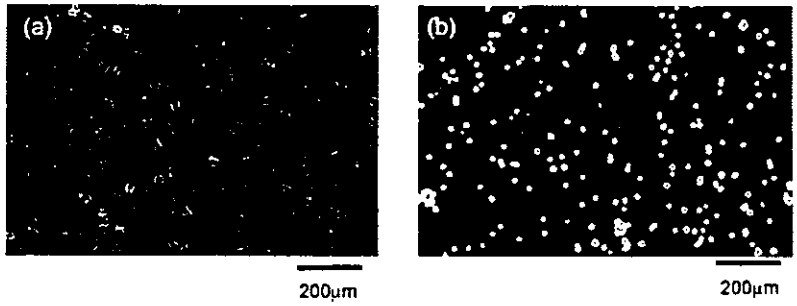

Figure 5. Phase-contrast microphotographs of bovine artery ECs cultured on PIPAAm-1.4 (a) and PIPAAm-2.9 (b) at 37 °C for 1 day.

Table 1. Properties of PIPAAm-1.4, PIPAAm-2.9, and PIPAAm-50[a]

		PIPAAm-1.4	PIPAAm-2.9	PIPAAm-50
density of grafted PIPAAm ($\mu g/cm^2$)		1.4 ± 0.1	2.9 ± 0.1	1080
contact angle (cos θ)	37 °C	0.20	0.35	0.65 (40 °C)
	20 °C	0.42	0.50	0.98 (10 °C)
thickness of the grafted PIPAAm (nm)		15.5 ± 7.2	29.3 ± 8.4	5000
cell attachment/detachment properties	37 °C	yes	no adhesion	no adhesion
	20 °C	yes		
amount of adsorbed FN (ng/cm^2)	37 °C	150 ± 50	UD	UD
	20 °C	UD	UD	UD

[a] UD: Undetectable. Glass coverslips were used as the base substrate of PIPAAm-50. Density and thickness of the grafted PIPAAm were measured in the dry state.

Cell attachment/detachment responses on PIPAAm-grafted surfaces are the key factor for noninvasive recovery of cell sheets for further applications of tissue and organ reconstruction. Here we examined cellular responses to these PIPAAm-grafted surfaces in terms of cell adhesion and detachment with temperature. ECs adhered and spread on the PIPAAm-1.4 dishes (Figure 5a), whereas those on PIPAAm-2.9 did not (Figure 5b). The latter tendency was also observed for PIPAAm-50 (data not shown). Adhered and proliferated cells on PIPAAm-1.4 surfaces were detached from the surfaces by reducing temperature below the PIPAAm's transition temperature in single cells and/or monolayer cell sheets depending on cell density on the surfaces. This phenomenon was consistent with a previous report.[8]

The properties of PIPAAm-1.4, -2.9, and -50 are summarized in Table 1. Taking the water contact angle of the PIPAAm-grafted surfaces at 37 °C into account, these results support that the PIPAAm-50 surfaces are likely to be the most hydrophilic among the three surfaces, although these surfaces exhibit hydrophilic/hydrophobic alterations by temperature. The hydrophobic/hydrophilic properties are influenced by the amount and thickness of the grafted PIPAAm. There should be an optimum content of grafted PIPAAm to exhibit cell adhesion and detachment regulation.

Discussion

In the present study, we utilized the UV laser ablation technique, TOF-SIMS, and AFM methods to estimate the thickness of the PIPAAm-grafted layer on TCPS to correlate with cell adhesion/detachment behavior. Chan et al.[19] showed that a laser fluence of the UV excimer laser above ca. 50 mJ/cm^2 influenced the contact angles of resulting polystyrene film surfaces due to chemical property changes and the formation of debris. The laser fluence at 10 and 20 mJ/cm^2 was used for the ablation of PIPAAm-grafted surfaces to attain exposure of TCPS, avoiding the debris formation and any chemical property changes of the resulting surfaces. This was confirmed with fluorescent images and TOF-SIMS results. Surface topology before and after the laser ablation was not altered, also indicating much less contamination with the debris.

In our previous reports, the configuration and resulting dynamic motion of the grafted PIPAAm chains significantly influenced surface wettability in response to temperature changes.[1,2] We prepared one-side fixed PIPAAm hydrogels with glass coverslips and investigated the temperature-dependent swelling/deswelling changes. Compared with nonfixed hydrogels of 500-μm-thick gels, swelling was significantly restricted for one-side fixed gels (unpublished data). We then compared the swelling behavior of one-side fixed gels having different gel thicknesses. The swelling ratio for the thinner gels was less than half of that for the fixed gels with double thickness. These results imply that the molecular motion of the fixed and cross-linked chains is dramatically restricted. Such influences may be significant in the vicinity of matrix surfaces. These considerations are extended to discuss the differences in surface property alterations with PIPAAm-grafted surfaces having different graft amounts. Figure 6 illustrates a schematic drawing of the differences in molecular motion of grafted PIPAAm chains on two types of PIPAAm-grafted surfaces at 20 and 37 °C. An arrow with a gradient of black color illustrates the degree of the molecular motion. The darker polymer chains represent more restricted molecular motion, while brighter chains are more mobile. In the case of the ultrathin PIPAAm gel layers on TCPS, hydrophobic interaction at TCPS interfaces (indicated as a black region between TCPS and PIPAAm chains) is also likely to promote aggregation and enhanced dehydration of the covalently bound PIPAAm chains. The hydrophobic and immobile TCPS interfaces restrict molecular motion of the PIPAAm grafted chains (darker networks in Figure 6). Such restriction of chain mobility should be extended to the outermost regions of PIPAAm chains for PIPAAm-1.4. Thus, PIPAAm-1.4 was relatively more hydrophobic

(19) Chan, C. M.; Ko, T. M.; Hiraoka, H. *Surf. Sci. Rep.* **1996**, *24*, 1–54.

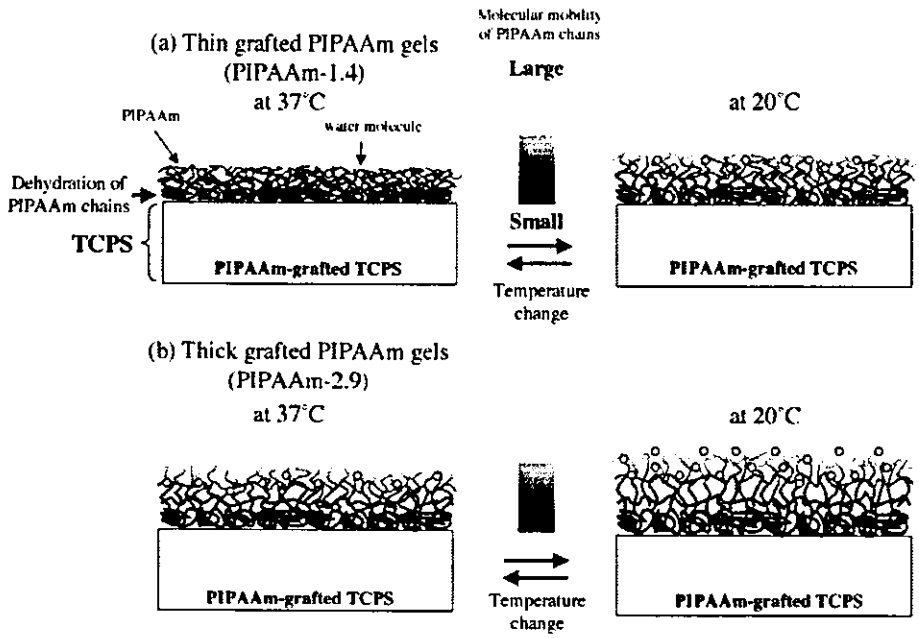

Figure 6. Schematic drawings of the influence of molecular motion of grafted PIPAAm chains on hydration of the polymer chains, when the grafted PPAAm gels are thin (a) and thick (b) at 20 °C (left side) and 37 °C (right side), respectively. Hydrophobic TCPS interfaces promoting aggregation and dehydration were represented as a black region in TCPS. Molecular motion of the grafted polymer chains becomes larger according to the distance away from TCPS interfaces.

than PIPAAm-2.9. For the thicker polymer grafted gel of PIPPAm-2.9, more polymer chains at the outermost regions are hydrated than those on PIPAAm-1.4-grafted surfaces (Figure 6b). In other words, as illustrated schematically in Figure 6b, more hydration for PIPAAm-2.9 surfaces should be occurring than for PIPAAm-1.4. Such changes greatly influence the contact angle changes and cell adhesion/detachment behavior. The observed cell adherent and nonadherent surface characteristic changes occur in only 15–20-nm differences for the examined surfaces. Membranes prepared by the solvent-cast method usually have thicknesses in the range of several micrometers. Such thicker PIPAAm-coated surfaces showed nonfouling characteristics to cells without addition of cell adhesion proteins such as collagen[20] and gelatin components.[21] Such a non-cell-adherent property is also seen for PIPAAm-50 (Table 1). Covalent bonds of the PIPAAm-50 gels on the solid glass coverslips resulted in the restricted molecular motion of the grafted polymer chains, inducing suppressed gel swelling. However, as was seen in Table 1, the outermost gel surfaces showed more polar characteristics than nanometer-thick PIPAAm gel grafted surfaces in terms of the surface wettability even at 37 °C. Electron beam irradiation polymerization is extremely essential for design of the nanometer-thick interfaces to regulate grafted PIPAAm thickness and the following cell adhesion/detachment control by temperature.

(20) Takezawa, T.; Mori, Y.; Yoshizato, K. *Bio/Technology (NY)*, **1990**, *8* (9), 854–856.
(21) Morikawa, N.; Matsuda, T. *J. Biomater. Sci., Polym. Ed.* **2002**, *13*, 167–184.

Conclusions

In the present study, we demonstrate that thickness and the amount of grafted PIPAAm layers have significant influence on surface properties in terms of thermoresponsive cell adhesion and detachment and approximately 20-nm thickness is the key factor for the PIPAAm-grafted surface to achieve adhesive cell adhesion and detachment with temperature. Progressive dehydration of PIPAAm chains existing at the vicinity of hydrophobic TCPS may be important to show cell adhesion character at 37 °C. By contrast, the graft polymer at the outermost interfaces of PIPAAm-2.9 should have more polar characteristics even at 37 °C than PIPAAm-1.4, which causes cells not to adhere on it.

Acknowledgment. This work was partly supported by a Grant-in-Aid for Scientific Research (Grant No. 13308055), the Japan Society for Promotion of Science (JSPS), and carried out under the Center of Excellence (COE) Program for 21st Century, "The Center for Tissue Engineering and Regenerative Medicine", the Ministry of Education, Culture, Sports, Science and Technology (MEXT), Japan.

LA036139F

FEBS Letters 565 (2004) 6–10 FEBS 28299

Human limbal epithelium contains side population cells expressing the ATP-binding cassette transporter ABCG2

Katsuhiko Watanabe[a], Kohji Nishida[a,*], Masayuki Yamato[b], Terumasa Umemoto[b], Taizo Sumide[a], Kazuaki Yamamoto[a], Naoyuki Maeda[a], Hitoshi Watanabe[a], Teruo Okano[b], Yasuo Tano[a]

[a]*Department of Ophthalmology, Osaka University Medical School, Room E7, Yamadaoka 2-2, Suita, Osaka 565-0871, Japan*
[b]*Institute of Advanced Biomedical Engineering and Science, Tokyo Women's Medical University, 8-1 Kawada-cho, Shinjuku-ku, Tokyo 162-8666, Japan*

Received 9 January 2004; revised 9 March 2004; accepted 9 March 2004

First published online 7 April 2004

Edited by Veli-Pekka Lehto

Abstract Many types of organ-specific stem cells have been recently shown to exhibit a side population (SP) phenotype based on their ability to efflux Hoechst 33342 dye. Because stem cells from corneal epithelium reside in the basal layer of the limbal epithelium, the purpose of this study was to examine whether the limbal epithelium contains SP cells. The ATP-binding cassette transporter Bcrp1/ABCG2 is reported to contribute to the SP phenotype in cells from several diverse sources. Here we show data from fluorescence-activated cell sorting and real-time quantitative RT-PCR analysis showing that harvested limbal epithelial cells contain SP cells expressing ABCG2. Immunofluorescence revealed that a portion of limbal epithelial basal cells expressed ABCG2. Data indicate that ABCG2 positive limbal epithelial cells are putative corneal epithelial stem cells.

Keywords: Corneal epithelium; Limbal epithelium; Stem cell; Side population; ABCG2

1. Introduction

The cornea – the transparent outer anterior tissue layer of the eye – provides the eye with protection and refractive properties essential for vision. These functions depend, in part, on the corneal epithelium, a highly specialized cell layer comprising both basal and stratified squamous cells. Corneal epithelial stem cells reside in the basal layer of the limbus [1,2], the transitional zone between the cornea and the more peripheral bulbar conjunctiva. These cells allow the renewal of the corneal epithelium by generating transient amplifying cells that migrate, proliferate and differentiate to replace lost corneal epithelial cells [3–5]. However, because of the absence of the definite biological markers, unequivocal corneal epithelial stem cell identification remains elusive.

In 1996, Goodell et al. [6] demonstrated that mouse hematopoietic stem cells with long-term multi-lineage reconstituting ability can be isolated as side population (SP) cells based on their ability to efflux the Hoechst 33342 dye. Using dual wavelength flow cytometric analysis, SP cells were identified as a distinct population with low Hoechst 33342 blue/red fluorescence representing approximately 0.1% of total bone marrow cells [6]. SP cells have also been identified in hematopoietic compartments in a number of animals [7–10]. In addition, SP cells have been isolated from various types of adult tissue where they demonstrate stem cell activity [6,10–16]. These findings suggest that the SP phenotype represents a common feature of stem cells.

Recently, Zhou et al. [13,17] reported that the ATP-binding cassette transporter Bcrp1/ABCG2 is a molecular determinant of the SP phenotype. A number of other studies in a wide variety of organs have also indicated that the SP phenotype is largely determined by the expression of Bcrp1/ABCG2 [13,15,18–20]. More recently, Mogi et al. [21] have shown by targeted gene ablation studies in mice that serine/threonine kinase Akt signaling modulates the SP phenotype by regulating the expression of Bcrp1/ABCG2.

At present, it remains unclear if corneal epithelial stem cells might exhibit the SP phenotype. We report our recent studies on human limbal epithelium, providing evidence that these cells contain SP cell subsets expressing ABCG2, implicating possible relationships between these SP cells and limbal stem cells.

2. Materials and methods

2.1. Cell preparation

Human corneoscleral rims from USA eye bank eyes were used. Limbal tissues were obtained by using scissors, and 8.0-mm diameter central portions of corneas were obtained by trephination. Limbal tissues and central corneas were incubated separately at 37 °C in Dulbecco's modified Eagle's medium (DMEM; Nikken Biomedical Laboratory, Kyoto, Japan) containing 2.4 units/ml dispase (Invitrogen, Carlsbad, CA) for 1 h. Epithelial cells were separated under a dissecting microscope and treated with 0.25% trypsin-1 mM EDTA solution (Invitrogen) for 15 min at 37 °C to achieve each single cell suspensions from the limbal epithelium and the corneal epithelium. Enzymatic activity was then stopped by adding an equal volume of DMEM containing 10% fetal calf serum (FCS; Morgate Biotech, Qld., Australia).

2.2. Hoechst 33342 dye exclusion assay

Separate populations of epithelial cells from the limbus and from the cornea were resuspended at 1.0×10^6 cells/ml in incubation medium

* Corresponding author. Fax: +81-6-6879-3458.
E-mail address: knishida@ophthal.med.osaka-u.ac.jp (K. Nishida).

0014-5793/$22.00
doi:10.1016/j.febslet.2004.03.064

(DMEM containing 2% FCS and 10 mM HEPES (Sigma)) and subsequently divided into two portions. After incubation in incubation medium for 90 min at 37 °C, (*R*)+-verapamil (Sigma, St. Louis, MO) or tryprostatin A (TPS-A; provided by Dr. H. Osada (RIKEN Institute)) was added to one portion (final concentration: 50 μM), after which both portions were incubated for a further 30 min at 37 °C. Antibody-mediated inhibition assay using anti-ABCG2 monoclonal antibody (5D3; eBioscience, San Diego, CA) or isotype control (mouse IgG_{2b}; eBioscience) was performed as previously described [22]. Hoechst 33342 dye (Sigma) was then added to both portions (final concentration: 3 μg/ml), and incubation continued for another 90 min at 37 °C. After the final incubation, cells were kept on ice and analyzed for Hoechst 33342 dye efflux by EPICS Altra FACS analysis (Beckman Coulter, Fullerton, CA). Prior to analysis, propidium iodide (Sigma) was added (final concentration: 2 μg/ml) to distinguish live from dead cells. Hoechst 33342 dye was excited at 350 nm using a UV laser. Fluorescence emission was detected through 450 nm BP (Hoechst blue) and 675 nm LP (Hoechst red) filters, respectively. Propidium iodide in cells was excited at 488 nm (argon ion laser) and fluorescence emission was detected through a 610 nm BP filter.

2.3. Real-time quantitative RT-PCR analysis

SP and non-SP cells were isolated from limbal epithelial cells using EPICS Altra flow cytometric sorting. Total RNA was obtained from equal numbers (2000–3000) of SP and non-SP cells according to the manufacturer's instructions (Isogen; Nippongene, Tokyo, Japan). After DNase I (Invitrogen) treatment, total cellular RNA was divided into two portions. One portion was reverse transcribed with oligo$(dT)_{12-18}$, according to the manufacturer's instructions (SuperScript First-Strand Synthesis System for RT-PCR; Invitrogen), and a 1/10 volume (2 μl) of synthesized cDNA was used as a template for PCR. The other portion was treated in the same manner except for the omission of SuperScript II reverse transcriptase (Invitrogen). The oligonucleotide primers (Invitrogen) used for ABCG2 amplification were 5′-GGTTTCCAAGCGTTCATTCAAA-3′ (forward) and 5′-TAGCCCAAAGTAAATGGCACCTA-3′ (reverse), with an expected product length of 111 bp. The TaqMan probe (Applied Biosystems, Foster City, CA) used for ABCG2 detection was 5′-CCCAGGCCTCTATAGCTCAGATCATTGTCA-3′, labeled with 6-carboxyfluorescein (FAM) at the 5′-end, and with 6-carboxytetraethylrodamine (TAMRA) at the 3′-end. Quantitative PCR was performed using ABI Prism 7900HT Sequence Detection System (Applied Biosystems), according to the manufacturer's instructions. The reaction mixture (30 μl) contained 15 μl of TaqMan Universal PCR Mastermix (Applied Biosystems), 15 pmol of forward and reverse primers, 7.5 pmol of TaqMan probe and 2 μl of the investigated sample. Glyceraldehyde-3-phosphate dehydrogenase (GAPDH) expression was measured using TaqMan GAPDH Control Reagents (Applied Biosystems), according to the manufacturer's instructions. Thermocycling used 50 cycles at 95 °C for 15 s and 60 °C for 1 min with an initial cycle at 50 °C for 2 min and 95 °C for 10 min. A negative control with non-reverse transcribed total RNA as a template was included in every experiment. All assays were run in duplicate. To represent the ABCG2 mRNA expression level, we used the ABCG2 mRNA expression index as the value of the ABCG2 gene copies divided by the value of the housekeeping GAPDH gene copies.

2.4. Statistical analysis

Statistics were calculated using SigmaStat 2.0 (SPSS, Chicago, IL). To compare ABCG2 expression between SP and non-SP cells, the Mann–Whitney rank sum test was applied.

2.5. Immunofluorescence

Cryostat sections (20 μm) were cut from the limbus and from the cornea, dried for 1 h at room temperature, and fixed in acetone for 10 min also at room temperature. Immunofluorescence was performed using DakoCytomation CSA II (DakoCytomation, Kyoto, Japan). Briefly, endogenous peroxidase activity was blocked with 3% hydrogen peroxide in water for 15 min. The slides were first incubated with serum-free protein in buffer for 15 min to block non-specific binding of antibodies, then incubated at 4 °C overnight with a 1:2500 dilution of BXP-21 monoclonal antibody (MBL, Aichi, Japan). BXP-21 was diluted in tris-buffered saline containing 1% bovine serum albumin and 0.1% Tween 20. After incubation, slides were incubated for 15 min with anti-mouse immunoglobulins-HRP, followed by 15 min in fluorescyl-tyramide hydrogen peroxide in buffer. After counterstaining with propidium iodide (Sigma), slides were mounted and observed on a confocal laser scanning microscope (LSM 510 META; Carl Zeiss, Jena, Germany). For each type of tissue, identically treated negative controls were included using normal non-specific IgG_{2a} (DakoCytomation).

3. Results

3.1. SP cells are present in human limbal epithelium

In the Hoechst 33342 dye exclusion assay, a distinct population of cells with a low Hoechst 33342 blue/red fluorescence was detected in epithelial cells from the limbus (Fig. 1A; 0.20% gated cells) but not in cells from the cornea (Fig. 1B, 1D; 0.02% gated cells). Generation of this subpopulation was not seen in the presence of (*R*)+-verapamil, the specific inhibitor of Hoechst 33342 dye transport (Fig. 1C; 0.01% gated cells). These observations indicate that the limbal epithelium contains SP cells.

3.2. Effect of 5D3 and TPS-A on Hoechst 33342 dye efflux

When SP cells were incubated with an anti-ABCG2 monoclonal antibody, 5D3, recognizing an external plasma membrane epitope on living cells [13,22], prior to Hoechst 33342 dye exclusion assay, a marked decrease in SP cell dye efflux was observed (Fig. 2A). Hoechst 33342 dye efflux activity was also inhibited by a novel ABCG2 inhibitor, TPS-A (Fig. 2B), that is known not to inhibit another important ATP-binding cassette transporter, P-glycoprotein [23]. These data strongly suggest that ABCG2 is a major contributor to the SP phenotype of limbal epithelial cells.

3.3. ABCG2 mRNA expression in SP and non-SP cells

To investigate the link between the SP phenotype and ABCG2 expression, SP and non-SP cells from limbal epithelial tissues were analyzed for ABCG2 gene expression by TaqMan real-time

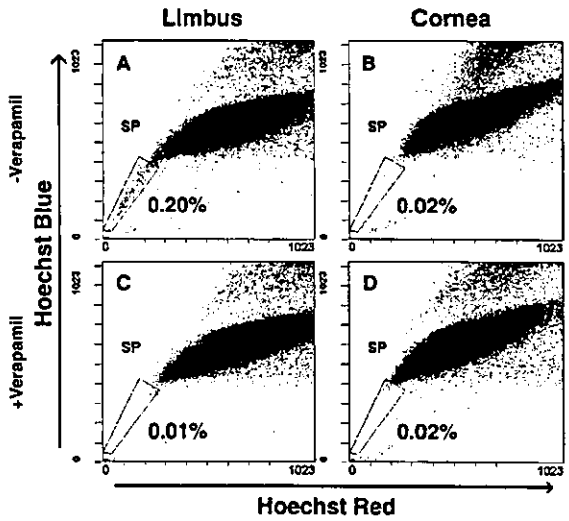

Fig. 1. Flow cytometric analysis of epithelial cells harvested from the limbus and from the cornea. Epithelial cells were isolated from eye bank limbus and cornea tissues, and analyzed for Hoechst 33342 dye efflux by FACS. (A) SP cells were detected in limbal epithelial cells after Hoechst 33342 dye staining. (B) SP cells were absent in corneal epithelial cells. (C) Dye efflux from SP cells was inhibited by verapamil. (D) Verapamil had no effect on dye efflux.

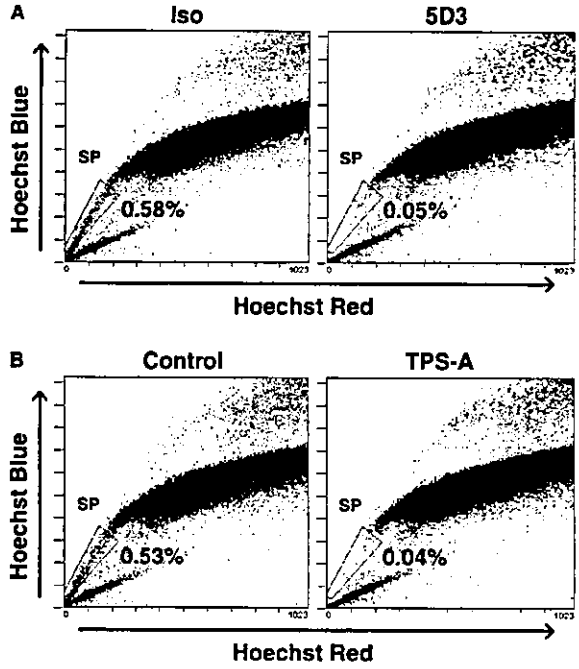

Fig. 2. Influence of ABCG2 inhibitors on the SP phenotype of limbal epithelial cells. Limbal epithelial cells were analyzed for Hoechst 33342 dye efflux in the presence of ABCG2 inhibitors. Dye efflux from SP cells was effectively inhibited by 5D3 monoclonal antibody (A) and by TPS-A (B).

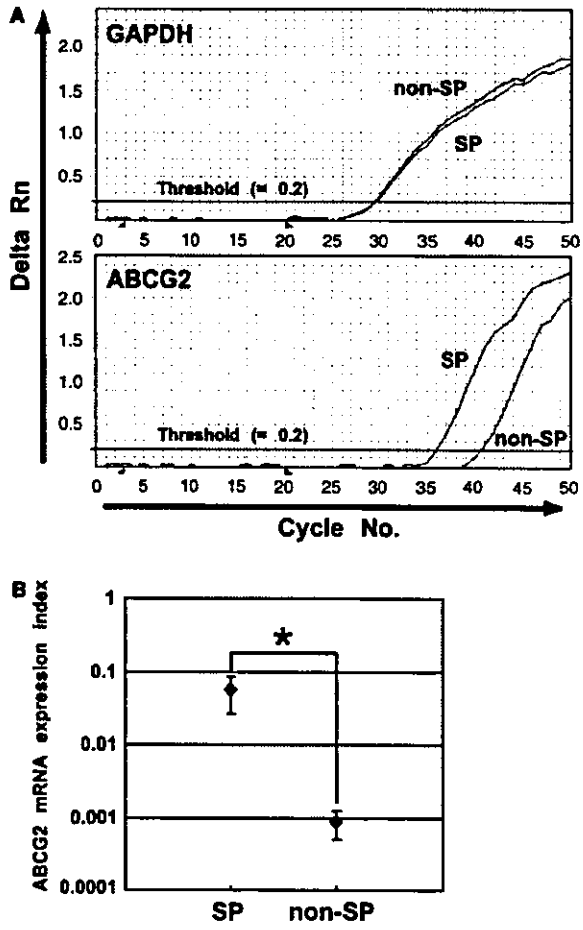

Fig. 3. Quantification of ABCG2 mRNA in SP and non-SP cells. (A) Amplification plots from real-time RT-PCR analysis. Delta Rn is plotted against cycle number. Horizontal red lines show the threshold used for calculation of ABCG2 expression indices. Real-time quantitative RT-PCR procedures were as described in Section 2. (B) ABCG2 mRNA expression indices in SP and non-SP cells. The relative expression of ABCG2 gene was normalized to that of GAPDH in each sample. Data represent the mean value from four samples. Error bars indicate the S.E. ABCG2 mRNA expression in SP cells was significantly higher than in non-SP cells ($P = 0.029$).

RT-PCR (Fig. 3A). ABCG2 mRNA expression indices were $5.61 \times 10^{-2} \pm 2.92 \times 10^{-2}$ (SP) and $8.66 \times 10^{-4} \pm 3.56 \times 10^{-4}$ (non-SP) ($n = 4$, mean ± S.E.) (Fig. 3B). Statistical analysis showed that the ABCG2 mRNA expression level in SP cells was significantly higher than in non-SP cells ($P = 0.029$).

3.4. Distribution of ABCG2-expressing cells

Our immunofluorescence data using BXP-21 monoclonal antibody specific for human ABCG2 revealed that ABCG2 is expressed in the limbal epithelial basal cells (Fig. 4A, B), but not in corneal epithelial cells (Fig. 4C). Observed ABCG2 expression in basal cells is inconsistent and discontinuous in the epithelium, and does not persist throughout the entire limbus (Fig. 4A). Fig. 4B shows that positive staining cells are present not only in the basal but also in the suprabasal cells.

4. Discussion

Corneal epithelial stem cell deficiency caused by ocular trauma or diseases causes corneal opacification and visual loss. Patients with corneal epithelial stem cell deficiency can be treated with autologous or allogenic limbal transplantation [24,25]. However, autologous limbal transplantation requires a large limbal withdrawal from the patient's eye, and allogenic limbal transplantation has a significant risk of rejection. Moreover, shortage of donor tissues is a serious current challenge. To avoid these problems, transplantations of cultivated corneal limbal epithelial cells have recently been reported [26–31]. In such tissue engineering approaches, development of new, effective methods for rapid identification and enrichment of corneal epithelial stem cells would be a considerable advantage since long-term, functional recovery of corneal epithelium is linked to graft constructs that retain viable stem cell populations [26,28,32].

In this study, we examined whether human limbal epithelium contains cells with SP phenotype, similar to stem cells in other organs [6,10–16]. Hoechst 33342 dye exclusion assays revealed that a number of SP cells are present in the limbal epithelium but not in the corneal epithelium (Fig. 1). The mean percentage of SP cells in limbal epithelial cells obtained from six independent experiments was calculated to be 0.29% (data not shown). This is a reasonable abundance value compared with that previously reported in other organs [6,10–16]. Though verapamil is generally used to identify the SP phenotype in the Hoechst 33342 dye exclusion assay, it is insufficient in specificity to demonstrate the contribution of ABCG2 to the SP phenotype of limbal epithelial cells. As ABCG2-specific inhibitors, fumitremorgin C [33], 5D3 monoclonal antibody

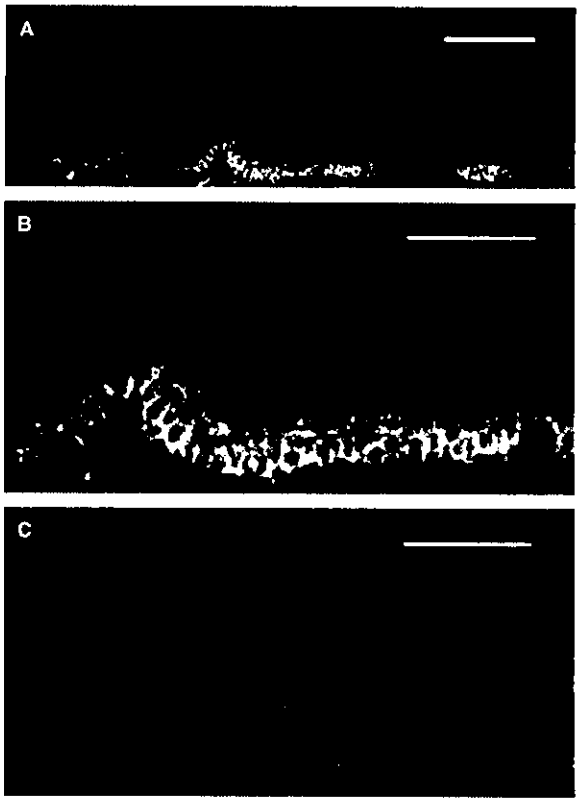

Fig. 4. Expression patterns of the ABCG2 marker using immunomarkers. Distribution of cells expressing ABCG2 protein was examined by immunofluorescence staining using the BXP-21 monoclonal antibody. (A) The basal layer of the limbal epithelium was inconsistently and discontinuously stained with anti-ABCG2 antibody (green). (B) A higher-magnification view of the limbal region showed that positively stained cells are present not only in the basal but also in the suprabasal cells. (C) ABCG2 was not expressed in the corneal epithelium. Nuclei were labeled with propidium iodide (red). Scale bar: 100 μm (A), 50 μm (B, C).

[13,22], and TPS-A [23] are reported. Our SP analysis of limbal epithelial cells using 5D3 and TPS-A showed that both 5D3 and TPS-A effectively inhibit Hoechst 33342 dye efflux from these cells (Fig. 2A, B). These data strongly suggest a correlation between SP phenotype and ABCG2 expression, but the possibility of partial contribution of other transporters to SP phenotype cannot be excluded. Real-time quantitative RT-PCR analysis showed a strong correlation between ABCG2 expression and the SP phenotype. The ABCG2 mRNA expression indices in SP and non-SP cells varied considerably between samples, but SP cells consistently expressed a significantly higher level of ABCG2 mRNA over non-SP cells (Fig. 3B). The variation observed in these experiments may be due to variable conditions of eye bank tissue samples affected by many uncontrolled factors including donor age, death-to-preservation time and tissue storage time.

Immunofluorescence work revealed that ABCG2 was inconsistently expressed within the basal layer of the limbal epithelium (Fig. 4A), but not in the corneal epithelium (Fig. 4C). These observations also indicated that ABCG2 positive cells are present not only in the basal but also in the suprabasal cells in some areas (Fig. 4B). This localization pattern for ABCG2-positive cells coincides almost identically with that for corneal epithelial stem cells demonstrated previously by several investigators [1,2,34–37]. These findings imply that ABCG2 positive cells in the limbal epithelium are putative corneal epithelial stem cells, consistent with the observation that SP cells are present in the limbal epithelium but not in the corneal epithelium (Fig. 1). Flow cytometry revealed that SP cells are only 0.20% of total limbal epithelial cells (Fig. 1A), but immunofluorescence showed that many more cells express ABCG2 (Fig. 4A, B). Because limbal epithelial basal cells have a small cytoplasmic volume, it is not clear whether ABCG2 molecules localize in the plasma membrane or in the cytoplasm (Fig. 4A, B). Since it has been reported that active ABCG2 is expressed on the surface of SP cells, and cytoplasmic ABCG2 cannot efflux Hoechst 33342 dye outside these cells [19,21,38,39], the smaller number of SP cells observed here can be explained by possible cytoplasmic localization of ABCG2. In addition, it is possible that our methods actually underestimate functional SP populations in limbal epithelial cells: cells were collected from eye bank eyes with varying death-to-preservation times and storage conditions, with the likelihood that viability, including dye efflux capability, might be reduced.

One possible biological function of ABCG2 expressed in the limbal epithelium is a protective function. Because Bcrp1/ABCG2 is known to transport a variety of toxic lipophilic compounds [40–42], ABCG2 may protect corneal epithelial stem cells from cytotoxic agents. Recently, Jonker et al. [43] found that Bcrp1/ABCG2-null mice become extremely sensitive to the dietary chlorophyll-breakdown product, pheophorbide a, resulting in severe, sometimes lethal, phototoxic lesions on light-exposed skin. This finding suggests that ABCG2 may protect corneal epithelial stem cells from solar damage. This is also consistent with the assertion that corneal epithelial stem cells are protected from solar damage by melanin pigmentation of the limbus in non-Caucasian people [2]. Another possibility is that ABCG2 may regulate the development of corneal epithelial stem cells by functioning as transporters of small hydrophobic regulatory molecules involved in proliferation, differentiation, or apoptotic pathways. However, the function of ABCG2 expressed in limbal epithelial basal cells remains a subject for further investigations.

In summary, our results suggest that the SP cell phenotype and cellular surface expression of ABCG2 may characterize putative corneal epithelial stem cells. Thus, ABCG2 may serve as a useful cell surface marker in the enrichment of viable corneal epithelial stem cells, and could be readily exploited for new tissue engineering approaches that attempt to reconstruct damaged ocular surfaces using cell transplantation methods.

Acknowledgements: We appreciate useful comments and technical criticism from Prof. D.W. Grainger (Colorado State University, USA) and Dr. A.J. Quantock (Cardiff University, UK). Dr. H. Osada (RIKEN Institute, Japan) provided TPS-A. The present work was supported in part by Grant-in Aid for Scientific Research (15390530) from the Ministry of Education, Culture, Sports, Science and Technology, Japan.

References

[1] Schermer, A., Galvin, S. and Sun, T.T. (1986) J. Cell Biol. 103, 49–62.
[2] Cotsarelis, G., Cheng, S.Z., Dong, G., Sun, T.T. and Lavker, R.M. (1989) Cell 57, 201–209.

[3] Kinoshita, S., Friend, J. and Thoft, R.A. (1981) Invest. Ophthalmol. Vis. Sci. 21, 434–441.
[4] Thoft, R.A. and Friend, J. (1983) Invest. Ophthalmol. Vis. Sci. 24, 1442–1443.
[5] Buck, R.C. (1985) Invest. Ophthalmol. Vis. Sci. 26, 1296–1299.
[6] Goodell, M.A., Brose, K., Paradis, G., Conner, A.S. and Mulligan, R.C. (1996) J. Exp. Med. 183, 1797–1806.
[7] Goodell, M.A., Rosenzweig, M., Kim, H., Marks, D.F., DeMaria, M., Paradis, G., Grupp, S.A., Sieff, C.A., Mulligan, R.C. and Johnson, R.P. (1997) Nat. Med. 3, 1337–1345.
[8] Storms, R.W., Goodell, M.A., Fisher, A., Mulligan, R.C. and Smith, C. (2000) Blood 96, 2125–2133.
[9] Uchida, N., Leung, F.Y. and Eaves, C.J. (2002) Exp. Hematol. 30, 862–869.
[10] Bhattacharya, S., Jackson, J.D., Das, A.V., Thoreson, W.B., Kuszynski, C., James, J., Joshi, S. and Ahmad, I. (2003) Invest. Ophthalmol. Vis. Sci. 44, 2764–2773.
[11] Jackson, K.A., Mi, T. and Goodell, M.A. (1999) Proc. Natl. Acad. Sci. USA 96, 14482–14486.
[12] Hulspas, R. and Quesenberry, P.J. (2000) Cytometry 40, 245–250.
[13] Zhou, S., Schuetz, J.D., Bunting, K.D., Colapietro, A.M., Sampath, J., Morris, J.J., Lagutina, I., Grosveld, G.C., Osawa, M., Nakauchi, H. and Sorrentino, B.P. (2001) Nat. Med. 7, 1028–1034.
[14] Asakura, A. and Rudnicki, M.A. (2002) Exp. Hematol. 30, 1339–1345.
[15] Lechner, A., Leech, C.A., Abraham, E.J., Nolan, A.L. and Habener, J.F. (2002) Biochem. Biophys. Res. Commun. 293, 670–674.
[16] Alvi, A.J., Clayton, H., Joshi, C., Enver, T., Ashworth, A., Vivanco, M.M., Dale, T.C. and Smalley, M.J. (2003) Breast Cancer Res. 5, R1–R8.
[17] Zhou, S., Morris, J.J., Barnes, Y., Lan, L., Schuetz, J.D. and Sorrentino, B.P. (2002) Proc. Natl. Acad. Sci. USA 99, 12339–12344.
[18] Kim, M., Turnquist, H., Jackson, J., Sgagias, M., Yan, Y., Gong, M., Dean, M., Sharp, J.G. and Cowan, K. (2002) Clin. Cancer Res. 8, 22–28.
[19] Scharenberg, C.W., Harkey, M.A. and Torok-Storb, B. (2002) Blood 99, 507–512.
[20] Shimano, K., Satake, M., Okaya, A., Kitanaka, J., Kitanaka, N., Takemura, M., Sakagami, M., Terada, N. and Tsujimura, T. (2003) Am. J. Pathol. 163, 3–9.
[21] Mogi, M., Yang, J., Lambert, J.F., Colvin, G.A., Shiojima, I., Skurk, C., Summer, R., Fine, A., Quesenberry, P.J. and Walsh, K. (2003) J. Biol. Chem. 278, 39068–39075.
[22] Abbott, B.L., Colapietro, A.M., Barnes, Y., Marini, F., Andreeff, M. and Sorrentino, B.P. (2002) Blood 100, 4594–4601.
[23] Woehlecke, H., Osada, H., Herrmann, A. and Lage, H. (2003) Int. J. Cancer 107, 721–728.
[24] Kenyon, K.R. and Tseng, S.C. (1989) Ophthalmology 96, 709–723.
[25] Tsubota, K., Satake, Y., Kaido, M., Shinozaki, N., Shimmura, S., Bissen-Miyajima, H. and Shimazaki, J. (1999) N. Engl. J. Med. 340, 1697–1703.
[26] Pellegrini, G., Traverso, C.E., Franzi, A.T., Zingirian, M., Cancedda, R. and De Luca, M. (1997) Lancet 349, 990–993.
[27] Tsai, R.J., Li, L.M. and Chen, J.K. (2000) N. Engl. J. Med. 343, 86–93.
[28] Rama, P., Bonini, S., Lambiase, A., Golisano, O., Paterna, P., De Luca, M. and Pellegrini, G. (2001) Transplantation 72, 1478–1485.
[29] Tseng, S.C., Meller, D., Anderson, D.F., Touhami, A., Pires, R.T., Gruterich, M., Solomon, A., Espana, E., Sandoval, H., Ti, S.E. and Goto, E. (2002) Adv. Exp. Med. Biol. 506, 1323–1334.
[30] Nishida, K. (2003) Cornea 22, S28–S34.
[31] Nishida, K., Yamato, M., Hayashida, Y., Watanabe, K., Maeda, N., Watanabe, H., Yamamoto, K., Nagai, S., Kikuchi, A., Tano, Y. and Okano, T. (2004) Transplantation 77, 379–385.
[32] Ti, S.E., Anderson, D., Touhami, A., Kim, C. and Tseng, S.C. (2002) Invest. Ophthalmol. Vis. Sci. 43, 2584–2592.
[33] Allen, J.D., van Loevezijn, A., Lakhai, J.M., van der Valk, M., van Tellingen, O., Reid, G., Schellens, J.H., Koomen, G.J. and Schinkel, A.H. (2002) Mol. Cancer Ther. 1, 417–425.
[34] Kurpakus, M.A., Stock, E.L. and Jones, J.C. (1990) Invest. Ophthalmol. Vis. Sci. 31, 448–456.
[35] Matic, M., Petrov, I.N., Chen, S., Wang, C., Dimitrijevich, S.D. and Wolosin, J.M. (1997) Differentiation 61, 251–260.
[36] Pellegrini, G., Dellambra, E., Golisano, O., Martinelli, E., Fantozzi, I., Bondanza, S., Ponzin, D., McKeon, F. and De Luca, M. (2001) Proc. Natl. Acad. Sci. USA 98, 3156–3161.
[37] Espana, E.M., Romano, A.C., Kawakita, T., Di Pascuale, M., Smiddy, R. and Tseng, S.C. (2003) Invest. Ophthalmol. Vis. Sci. 44, 4275–4281.
[38] Rocchi, E., Khodjakov, A., Volk, E.L., Yang, C.H., Litman, T., Bates, S.E. and Schneider, E. (2000) Biochem. Biophys. Res. Commun. 271, 42–46.
[39] Summer, R., Kotton, D.N., Sun, X., Ma, B., Fitzsimmons, K. and Fine, A. (2003) Am. J. Physiol. Lung. Cell. Mol. Physiol. 285, L97–L104.
[40] Allen, J.D., Brinkhuis, R.F., Wijnholds, J. and Schinkel, A.H. (1999) Cancer Res. 59, 4237–4241.
[41] Jonker, J.W., Smit, J.W., Brinkhuis, R.F., Maliepaard, M., Beijnen, J.H., Schellens, J.H. and Schinkel, A.H. (2000) J. Natl. Cancer Inst. 92, 1651–1656.
[42] Robey, R.W., Medina-Perez, W.Y., Nishiyama, K., Lahusen, T., Miyake, K., Litman, T., Senderowicz, A.M., Ross, D.D. and Bates, S.E. (2001) Clin. Cancer Res. 7, 145–152.
[43] Jonker, J.W., Buitelaar, M., Wagenaar, E., Van Der Valk, M.A., Scheffer, G.L., Scheper, R.J., Plosch, T., Kuipers, F., Elferink, R.P., Rosing, H., Beijnen, J.H. and Schinkel, A.H. (2002) Proc. Natl. Acad. Sci. USA 99, 15649–15654.

TISSUE ENGINEERING
Volume 10, Number 7/8, 2004

Immobilization of Cell-Adhesive Peptides to Temperature-Responsive Surfaces Facilitates Both Serum-Free Cell Adhesion and Noninvasive Cell Harvest

MITSUHIRO EBARA,[1] MASAYUKI YAMATO, Ph.D.,[2] TAKAO AOYAGI, Ph.D.,[2] AKIHIKO KIKUCHI, Ph.D.,[2] KIYOTAKA SAKAI, Ph.D.,[1] and TERUO OKANO, Ph.D.[2]

ABSTRACT

We have developed temperature-responsive cell culture surfaces to harvest intact cell sheets for tissue-engineering applications. Both cost and safety issues (e.g., prions, bovine spongiform encephalopathy) are compelling reasons to avoid use of animal-derived materials, including serum, in such culture. In the present study, synthetic cell-adhesive peptides are immobilized onto temperature-responsive polymer-grafted surfaces, and cell adhesion and detachment under serum-free conditions were examined. The temperature-responsive polymer poly(*N*-isopropylacrylamide) (PIPAAm) was functionalized by copolymerization with a reactive comonomer having both a carboxyl group and an isopropylacrylamide group. These copolymers were covalently grafted onto tissue culture-grade polystyrene dishes. Synthetic cell-adhesive peptides were then immobilized onto these surfaces via carboxyl groups. Bovine aortic endothelial cells both adhered and spread on these surfaces even under serum-free conditions at 37°C, similar to those in 10% serum-supplemented culture. Spread cells promptly detached from the surfaces on lowering culture temperatures below the lower critical solution temperature of the polymer, 32°C. These surfaces would be useful for serum-free culture for tissue-engineering applications.

INTRODUCTION

WE HAVE DEVELOPED temperature-responsive culture dishes on which various cell types adhere and multiply similarly to cells on tissue culture polystyrene (TCPS) dishes at 37°C. On these surfaces, spread cells spontaneously detach on reduction of the culture temperature below the polymer's lower critical solution temperature (LCST, 32°C), as a result of rapid hydration of the grafted dish polymer surface.[1,2] When the culture temperature is reduced after cells reach confluency, all cells are harvested as a single contiguous cell sheet.[3,4] These transplantable cell sheets retain cell–cell junctional proteins as well as intact extracellular matrix underneath the cell sheets.[3,5,6] Furthermore, cell function is often maintained: harvested pulsating cardiac myocyte sheets become stratified *in vitro*,[7] and can be grafted *in vivo*.[8] Histological and functional integration of cardiac myocyte sheets is shown after culture stratification and tissue grafting. Therefore, we currently utilize the culture method for tissue-engineering applications.

Both cost and safety issues in cell culture argue for the development of cell culturing, harvesting, and device construction methods that require no mammalian-sourced

[1]Department of Applied Chemistry, Waseda University, Tokyo, Japan.
[2]Institute of Advanced Biomedical Engineering and Science, Tokyo Women's Medical University, Tokyo, Japan.

components. For example, cell culture reagents are often sourced from bovine serum at considerable expense, and the risk of cross-infecting humans with bovine pathogens (viruses, prions, and spongiform encephalopathy in Europe and Japan) is a concern.[9,10] Because temperature-responsive culture dishes require cell-adhesive proteins for cell adhesion and spreading, like tissue culture polystyrene (TCPS), serum or cell-adhesive proteins such as fibronectin derived from serum are commonly utilized. To achieve serum-free culture in the present study, the common synthetic cell adhesive peptide Arg-Gly-Asp-Ser (RGDS)[11,12] was immobilized on temperature-responsive culture dishes on which copolymers of *N*-isopropylacrylamide (IPAAm) and 2-carboxyiso-propylacrylamide (CIPAAm)[13] had been covalently grafted. This surface affords adhesion, culture, and harvest of cell sheets under serum-free conditions.

MATERIALS AND METHODS

Materials

N-Isopropylacrylamide (IPAAm) was kindly provided by Kohjin (Tokyo, Japan) and purified by recrystallization from *n*-hexane. 2-Carboxyisopropylacrylamide (CIPAAm) was synthesized as described previously.[13] Acrylic acid (AAc) was purchased from Wako Pure Chemicals (Tokyo, Japan) and distilled under reduced pressure. TCPS dishes (Falcon 3001) were purchased from BD Biosciences Discovery Labware (Oxnard, CA). Synthetic cell-adhesive peptides were purchased from Sigma (St. Louis, MO). 1-Ethyl-3-(3-dimethylaminopropyl)-carbodiimide hydrochloride (water-soluble carbodiimide; WSC) was purchased from Dojindo Laboratories (Kumamoto, Japan). Bovine aortic endothelial cells (BAECs) were provided by

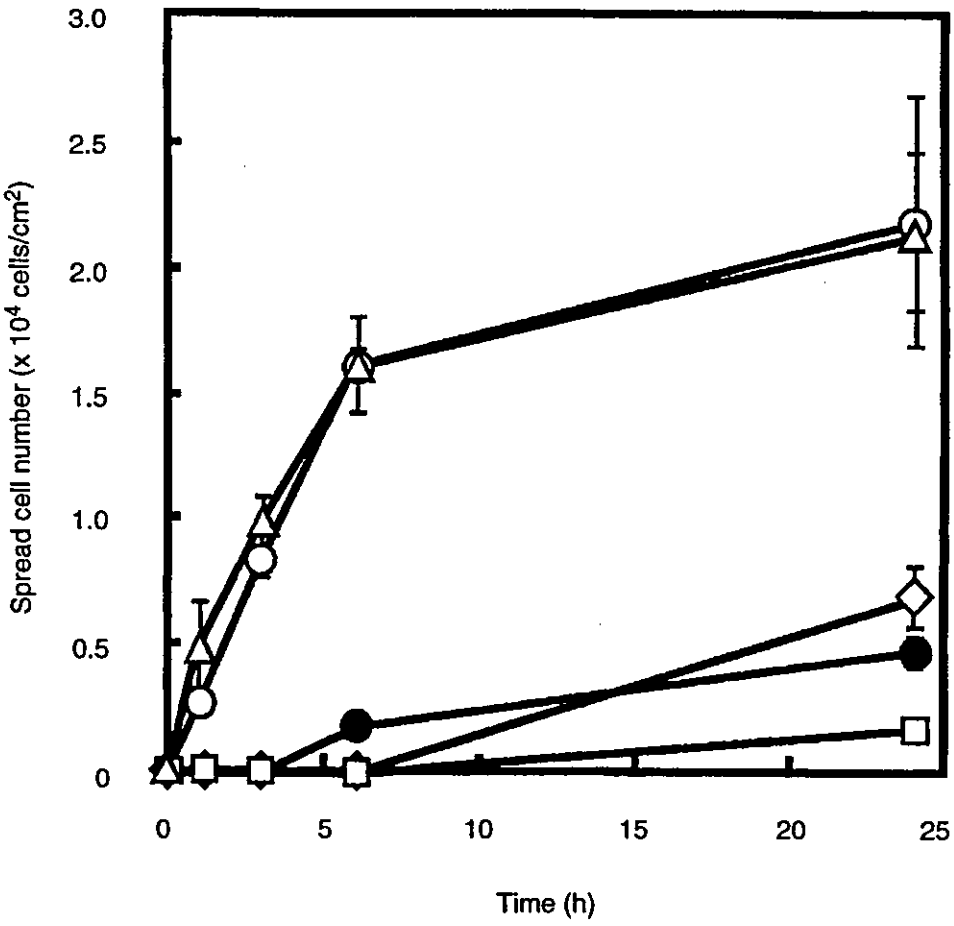

FIG. 1. BAEC spreading on RGDS-immobilized temperature-responsive culture surfaces. RGDS peptides were covalently grafted on P(IPAAm-*co*-CIPAAm)-grafted surfaces (IPAAm: CIPAAm, 99:1 in feed). The feed concentration of RGDS peptides was 0 [RGDS(0)-IC(1), solid circles], 0.2 [RGDS(0.2)-IC(1), open circles], 1 [RGDS(1)-IC(1), triangles], and 2 mM [RGDS(2)-IC(1), squares]. BAEC spreading was examined without serum at 37°C.

the Health Science Research Resources Bank (JCRB 0099; Osaka, Japan). Trypsin–EDTA solution, streptomycin, and penicillin were purchased from GIBCO-BRL (Grand Island, NY). Dulbecco's modified Eagle's medium (DMEM) was purchased from Iwaki (Chiba, Japan). EGM-2 (growth factor supplements) was purchased from Cambrex BioScience Walkersville, (Walkersville, MD).

Grafting of temperature-responsive polymer and RGDS immobilization

Temperature-responsive polymer-grafted surfaces were prepared as described previously.[4,14] Briefly, IPAAm and carboxylic monomer CIPAAm were dissolved in 2-propanol at a total concentration of 55% (w/w) and 30-μL aliquots were spread uniformly over 35-mm TCPS dishes. These solutions contained different concentrations of CIPAAm (1–10 mol%). Then, electron beam irradiation using an area beam electron-processing system (Curetron EBC-200-AA2; Nissin High Voltage, Kyoto, Japan) at a radiation dose of 0.3 MGy promoted polymerization and covalent grafting of copolymer onto TCPS surfaces. After rinsing and drying, 1 mL of Dulbecco's phosphate-buffered saline (PBS; pH 7.4) containing both RGDS peptides (0.2, 1 and 2 mM) and carbodiimide coupling reagent, WSC (the same concentration of peptides), was spread over each surface at room temperature. After 1 day of incubation, these dishes were rinsed with distilled water and sterilized with ethylene oxide after drying. These RGDS-immobilized P(IPAAm-*co*-CIPAAm)-grafted TCPS surfaces were abbreviated as RGDS(X)-IC(Y), where X is the feed RGDS concentration (millimolar) and Y is the mole percentage of carboxyl-containing monomer groups in the feed.

Cell adhesion and spreading assay in culture

BAECs were expanded on TCPS dishes with DMEM supplemented with 10% fetal bovine serum (FBS), penicllin (100 units/mL), and streptomycin (100 μg/mL) at 37°C in a humidified atmosphere with 5% CO2. BAECs were harvested from TCPS dishes with 0.25% trypsin–0.26 mM EDTA in PBS. DMEM without serum was added, and the cells were centrifuged and resuspended in DMEM without serum. A fixed number of cells (2×10^4 cells/cm^2) was plated onto peptide-immobilized surfaces and cultured at 37 or 20°C. Cell morphology was monitored and photographed under a phase-contrast microscope (TE300; Nikon, Tokyo, Japan) at various times. The cell number was also counted on printed photographs and averaged ($n = 3$). The spread area of individual cells on each surface was determined by tracing the outline of each cell and integrating this area with NIH Image (version 1.62) software for the Macintosh. Spread cell number and cell area are presented as means ± standard deviation ($n = 3$).

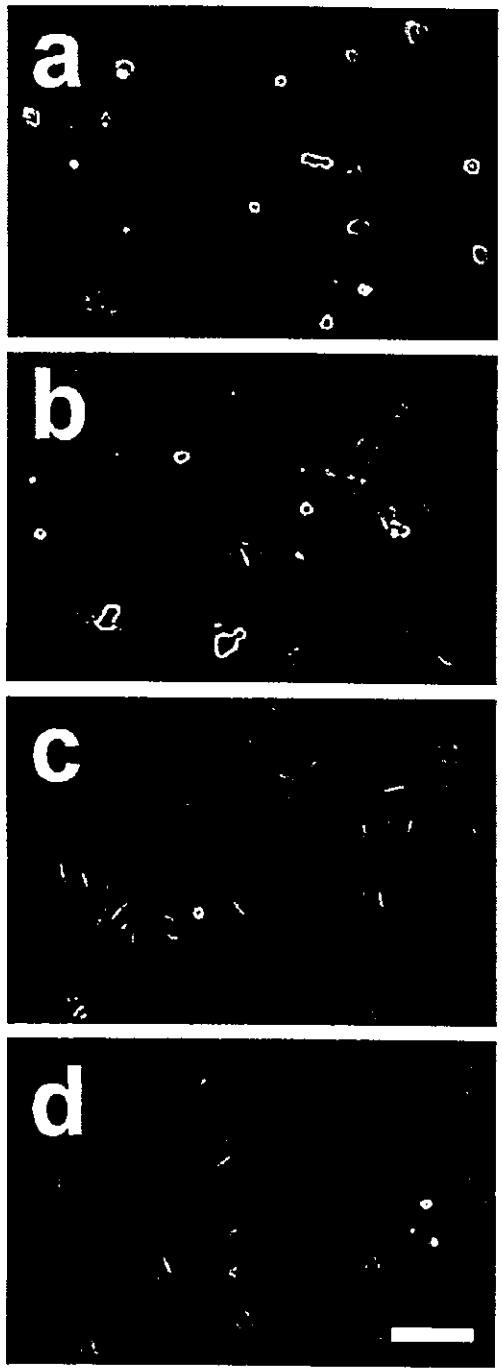

FIG. 2. Phase-contrast photographs of BAECs on RGDS-immobilized temperature-responsive culture surfaces. Representative cell morphologies after 24 h of culture without serum at 37°C are shown. (**a**) RGDS(0)-IC(1); (**b**) RGDS(0.2)-IC(1); (**c**) RGDS(1)-IC(1); (**d**) RGDS(2)-IC(1). Scale bar: 100 μm.

Cell detachment assay

Cell detachment from peptide-immobilized surfaces, done by reducing the cell culture temperature, was examined. BAECs were seeded sparsely (2.0×10^4 cells/cm^2) and densely (2.0×10^5 cells/cm^2) for the single-cell detachment assay and cell sheet detachment assay, respectively. For the single-cell detachment assay, BAECs were cultured for 24 h at 37°C. Culture medium was serum-free DMEM supplemented only with antibiotics. For the cell sheet detachment assay, BAECs were cultured for 1 week at 37°C. Culture medium was serum-free DMEM supplemented with antibiotics and EGM-2 containing human fibroblast growth factor B (hFGF-B), vascular endothelial growth factor (VEGF), recombinant insulin-like growth factor I (LongR^{3}IGF-I; Cell Sciences, Canton, MA), ascorbic acid, heparin, human epidermal growth factor (hEGF), hydrocortisone, gentamicin/amphotericin B (GA-1000) and lacking FBS. Dishes were then transferred to a CO_2 incubator equipped with a cooling unit fixed at 20°C to induce detachment by polymer surface swelling. Photomicrographs were taken at various times. The spread cell number was presented as means ± standard deviation (n = 3).

RESULTS

Cell adhesion on RGDS-immobilized temperature-responsive culture surfaces

Cell spreading was examined on synthetic cell-adhesive RGDS-immobilized surfaces under serum-free conditions. Increasing the peptide feed amounts increased cell spreading significantly in a dose-dependent manner (Fig. 1). Even on surfaces without immobilized peptides, scarce cell spreading was observed after 24 h of culture at 37°C, and this seemed to result from cell-secreted cell adhesion molecules. When the PIPAAm-grafted surfaces lacking carboxyl groups were subjected to similar blank peptide immobilization reactions with cell-adhesive pep-

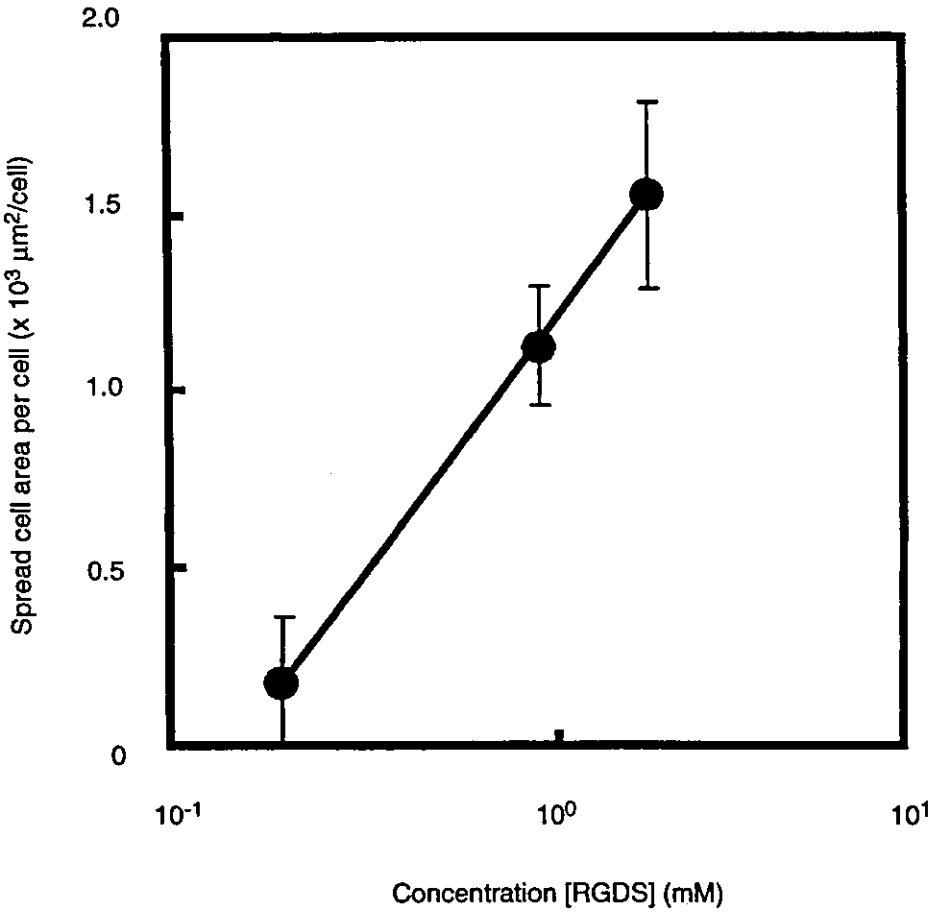

FIG. 3. Spread areas of individual BAECs on RGDS-immobilized temperature-responsive culture surfaces. Cell area on RGDS(0.2)-IC(1), RGDS(1)-IC(1), and RGDS(2)-IC(1) was measured after 24 h of culture without serum at 37°C, and plotted against the feed concentration of RGDS peptides.

tides, a similar basal level of cell spreading was observed in serum-free medium (data not shown). The total area of each cell was evaluated (Figs. 2 and 3). BAECs exhibited less spreading on surfaces immobilized with lesser amounts of cell-adhesive peptides. By increasing the peptide density, cells exhibited highly spread morphologies. Interestingly, cell spreading enhancement correlated well with the logarithm of the feed amount of cell-adhesive peptides (Fig. 3).

BAEC spreading was also examined on surfaces having various feed compositions of carboxyl comonomer groups, RGDS(2)-IC(*Y*), with a fixed (2 mM) feed of cell-adhesive peptide (Fig. 4). With increasing CIPAAm amounts, the spread cell number increased. Under optimized conditions of cell-adhesive peptide immobilization, RGDS(2)-IC(1), BAEC spreading in serum-free culture was the same as that observed on RGDS(0)-IC(1) in 10% FBS-supplemented DMEM (Fig. 5). On the other hand, BAEC spreading improvement was insignificant on a grafted RGDS(2)-IA(1) surface containing another comonomer, AAc, in place of CIPAAm under identical conditions. Cell spreading on RGDS(2)-IA(1) after 24 h of serum-free culture at 37°C was ~33% of that on RGDS(2)-IC(1). To confirm that the observed enhancement of cell attachment is mediated by immobilized RGDS peptides, competition assays were performed (Fig. 5). BAECs were suspended in serum-free DMEM containing RGDS peptides (50 μM) and incubated for 15 min at 37°C. These cells were then plated onto RGDS(*X*)-IC(1) and incubated at 37°C under serum-free conditions. Preincubation with soluble synthetic cell-adhesive peptides resulted in diminished cell spreading because RGDS peptides occupied cell membrane integrin, extracellular matrix receptors during the preincubation. Cell spreading was also considerably reduced when cells were seeded onto these surfaces at 20°C below the surface LCST.

Addition of growth factor supplements and high-density cell seeding allow cells to grow and reach confluency on RGDS(2)-IC(1) without serum (Fig. 6). RGDS

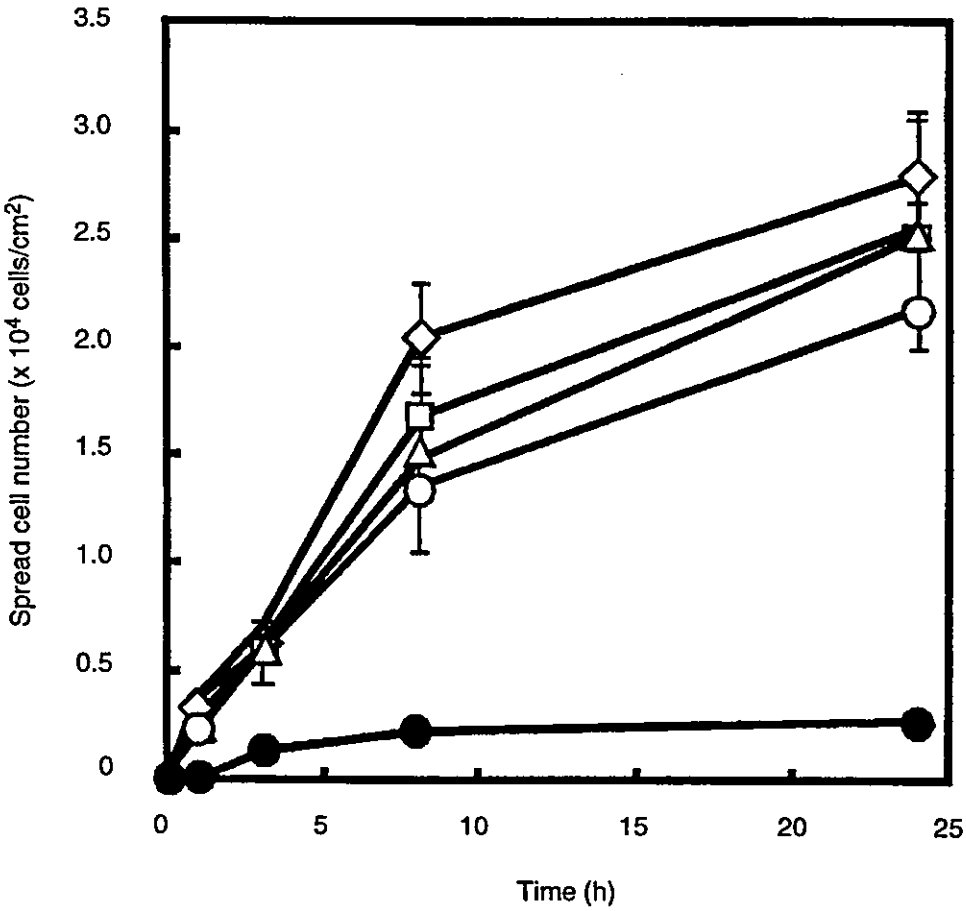

FIG. 4. BAEC spreading on RGDS-immobilized surfaces with various feed concentrations of CIPAAm comonomer. Temperature-responsive culture surfaces were prepared with various feed ratios of CIPAAm. RGDS peptides were then covalently grafted onto the surfaces. Feed concentrations of CIPAAm were 0 (solid circles), 1 (open circles), 3 (triangles), 5 (squares), and 10 mol% (diamonds). BAEC spreading was examined without serum at 37°C.